Determination of Failure Criteria for Suspended Ceiling Tile Systems and Thermal Resistance Provided Prior to Failure

by

Aidan C. Blanchard

Submitted in partial fulfilment of the requirements
for the degree of Master of Applied Science

at

Dalhousie University
Halifax, Nova Scotia
April 2022

DEDICATION

First, I would like to dedicate this research to both my parents who have done nothing but love and support me throughout my academic career. Secondly, to my mentors and friends who have endured with me throughout the course of this process. Finally, to the human understanding of fire. From the light in our caves to a destructive natural force, fire has played a significant role throughout the entirety of human history.

TABLE OF CONTENTS

LIST OF TABLES v
LIST OF FIGURES vi
ABSTRACT x
LIST OF ABBREVIATIONS USED xi
ACKNOWLEDGEMENTS xii
CHAPTER 1 INTRODUCTION 1
1.1 MOTIVATION 1
1.2 OBJECTIVES 1
1.3 SCOPE OF RESEARCH 1
1.4 SUMMARY OF CHAPTERS 2
CHAPTER 2 BACKGROUND 4
2.1 RATED AND NON-RATED CEILING TILE SYSTEMS 4
2.2 COMPLIANCE WITH BUILDING CODES 6
2.3 FIRE DYNAMICS SIMULATOR 9
CHAPTER 3 LITERATURE REVIEW 13
3.1 FIRE PERFORMANCE OF SUSPENDED CEILING TILE SYSTEMS 13
3.2 HEAT TRANSFER 14
3.3 METHODS 18
CHAPTER 4 APPARATUS DESIGN 21
4.1 APPARATUS FRAME 24
4.2 APPARATUS WALLS 24
4.3 ADJUSTABLE PLATFORM 25
4.4 SMOKE EXHAUST SYSTEM 26
4.5 CEILING TILE MATERIAL PROPERTIES 27
CHAPTER 5 EXPERIMENTAL SETUP 29
5.1 CEILING TILE ARRAY 29
5.2 HEAT SOURCE 30
5.3 HEAT SOURCE LOCATION 33
5.4 TEMPERATURE MEASUREMENT 33
5.4.1 K-Type Sheathed Thermocouples 33
5.4.2 K-Type Surface Thermocouples 34
5.4.3 Copper Plate Disk Thermometers 35
5.4.4 Location of Thermocouples 36
CHAPTER 6 EXPERIMENTAL DESIGN 38
6.1 BASIS FOR EXPERIMENTAL DESIGN 38
6.2 EXPERIMENTAL PARAMETERS 39
6.3 SEQUENCE OF TESTING 40
CHAPTER 7 RESULTS AND ANALYSIS 42
7.1 OVERVIEW OF TEST RESULTS 42

7.1.1 Observed Temperatures During Tests 42
7.1.2 Time to Failure 46
7.1.3 Endpoint Condition of Tiles 49
7.2 THERMAL RESISTANCE PROVIDED PRIOR TO FAILURE 53
7.2.1 Surface Temperature Distributions 53
7.2.2 Average Gas Temperatures 59
7.2.3 Heat Transfer Through Tiles 62
7.3 OBSERVED TEMPERATURES AT BURNER LOCATION 66
CHAPTER 8 NUMERICAL STUDY 69
8.1 DESCRIPTION OF MODEL 69
8.2 SENSITIVITY ANALYSIS 72
8.3 COMPARISON BETWEEN TESTING AND MODEL 74
CHAPTER 9 CONCLUSIONS AND RECOMMENDATIONS 79
9.1 SUMMARY 79
9.2 CONCLUSIONS 80
9.3 RECOMMENDATIONS 82
REFERENCES 84
APPENDIX A FDS SOURCE CODE 86

LIST OF TABLES

Table 1 Material properties of Armstrong® 902A MR acoustical ceiling tile panels. 28

Table 2 Outline of testing sequence detailing which parameter values were used in each replicate. 41

Table 3 Failure results for each test and the average times to failure (where observed). 47

Table 4 Calculated heat release rate, Q (kW), through the NCTS averaged from 447–477 seconds for each test, compared against the burner heat release rate. 64

Table 5 Results of sensitivity analysis for the initial, improved, and final meshes. 73

Table 6 Average model calculated surface temperatures after time of 60s. 75

Table 7 Average experimental surface temperatures after time of 60s. 75

LIST OF FIGURES

Figure 1 Sample visualization of FDS model. Courtesy of RJ Bartlett Engineering Ltd Report "12070 Final FPE Analysis R140327" [9] 10

Figure 2 "Figure 1. Schematic picture of the experimental system" as presented in Kokkala's Experimental Study of Heat Transfer to Ceiling from an Impinging Diffusion Flame [23]. 19

Figure 3 Conceptual image of the testing apparatus. 22

Figure 4 Image of the testing apparatus identifying individual components and systems. 23

Figure 5 Testing apparatus frame and cavity space. 24

Figure 6 Cement board walls of the apparatus, as viewed from the interior. 25

Figure 7 Adjustable platform surface and heat source within the apparatus. 26

Figure 8 Smoke exhaust system with apparatus removed except for the adjustable platform framing. 27

Figure 9 Ceiling tile arrangements tested as part of this research, as viewed from above/below: (a) four 610 mm × 610 mm tiles; and (b) two 610 mm × 1 220 mm tiles. 29

Figure 10 Installed (a) four-tile and (b) two-tile arrangements, viewed from below. 30

Figure 11 Cavity space above the ceiling tiles for an installed four-tile arrangement. 30

Figure 12 Schematic representation of the heat source used during experiments including fuel supply, means of measurement, and location of the burner relative to the location of the ceiling tiles array. 31

Figure 13 Propane burner in operation at a heat release rate of 13.5 kW with flame impingement on the ceiling tile system. 32

Figure 14 Cross-sectional view of a ceiling tile showing the installation of a copper disk plate thermometer. 36

Figure 15 Type, number, and location of thermocouples used to measure temperature above and below each tile. 37

Figure 16 Burner locations used during experiments shown relative to each ceiling tile arrangement used for (a) four 610 mm x 610 mm tiles; and (b) two 610 mm x 1 220 mm tiles. 40

Figure 17 Temperatures observed during testing: (a) Test 1; (b) Test 2; (c) Test 3 with sample of unexposed side surface thermocouple delamination; and (d) Test 4. 43

Figure 18 Temperatures observed during testing: (e) Test 5; (f) Test 6 with sample of propane auto shut-off; (g) Test 7 with sample of flow adjustment; (h) Test 8 with sample of unexposed side surface thermocouple delamination; (i) Test 9; and (j) Test 10. 44

Figure 19 Examples of flame breakthrough, taken from (a) Test 3 prior to failure; (b) Test 3 after failure; (c) Test 6 prior to failure; and (d) Test 6 after failure. 46

Figure 20 Endpoint condition of NCTS where failure was observed during testing: (a) Test 1; (b) Test 3; (c) Test 4; and (d) Test 6. 49

Figure 21 Side view of NCTS where failure was observed demonstrating sagging of the ceiling tile material for (a) Test 4; and (b) Test 6. 50

Figure 22 Endpoint condition of ceiling tiles where failure was not observed during testing: (a) Test 2; (b) Test 5; (c) Test 7; (d) Test 8; (e) Test 9; and (f) Test 10 51

Figure 23 Endpoint condition of the NCTS from Test 2, with the delicate areas of the tile removed using minimal force by a pen. 52

Figure 24 Surface temperatures observed prior to failure averaged from 447–477 seconds (with error bars representing one standard deviation) for (a) Test 1; (b) Test 2; (c) Test 3; and (d) Test 4. 54

Figure 25 Surface temperatures observed prior to failure averaged from 447–477 seconds (with error bars representing one standard deviation) for (e) Test 5; (f) Test 6; (g) Test 7; (h) Test 8; (i) Test 9; and (j) Test 10. 55

Figure 26 Log-Log plot of the observed temperature increase above ambient for all tests averaged from 447–477 seconds against radial distance from the centreline of the burner. 57

Figure 27 Temperature differences between the exposed and unexposed sides of the tiles averaged from 447–477 seconds (with error bars representing one standard deviation) for (a) tests at a height of 500 mm and (b) tests at a height of 250 mm. 58

Figure 28 Average temperature differences over the entire tile area between the exposed and unexposed sides of the tiles averaged from 447–477 seconds compared for each burner height and location. Mean values are represented by an "×", outlying data points are noted by the outer bounds, and the box represents the first through third quartile of data points. 59

Figure 29 Average gas temperatures on the exposed and unexposed sides of the tiles averaged from 447–477 seconds (with error bars representing one standard deviation) for each test. 60

Figure 30 Average gas temperature differences over the entire tile area between the exposed and unexposed sides of the tiles averaged from 447–477 seconds compared for each burner height and location. Mean values are represented by an "×", outlying data points are noted by the outer bounds, and the box represents the first through third quartile of data points. 61

Figure 31 Calculated heat flux, q'' (kW m-2), through the tiles as a function of radius at a time of 477 seconds for (a) tests at a height of 500 mm and (b) tests at a height of 250 mm. 63

Figure 32 Representation of discretized areas used as part of an integration-by-parts to calculate heat transfer through the NCTS for burner locations (a) at the centre; (b) right rear; and (c) right centre of the apparatus. 64

Figure 33 Average calculated rates of heat transfer through the NCST averaged from 447–477 seconds compared for each burner height and location. Mean values are represented by an "×", outlying data points are noted by the outer bounds, and the box represents the first through third quartile of data points. 65

Figure 34 Observed surface temperatures at r = 0.0 m at failure or, where failure was not observed, a time of 689 s (with error bars representing one standard deviation). Outlying data points are identified with a hollow marker. 67

Figure 35 Observed surface temperatures at r = 0.0 m at failure or, where failure was not observed, at the end of the testing period (with error bars representing one standard deviation). Outlying data points are identified with a hollow marker. 67

Figure 36 Sample image of Pyrosim model of Test 3 and Pyrosim user interface. A red surface represents the heat source with individual devices represented by yellow spheres. 70

Figure 37 Location of meshes having a grid size of (a) 20 mm and (b) 40 mm. 71

Figure 38 Temperatures observed in the (a) FDS model of Test #3 and (b) the physical results of Test #3..... 74

Figure 39 Comparison between (a) the observed fire plume during Test 3 and (b) visual representation of the visual fire plume as represented by Smokeview..... 76

Figure 40 Model calculated temperatures plotted against the observed temperatures for Test #3. Trendlines are provided for each the surface and gas temperatures on both the exposed and unexposed sides..... 77

ABSTRACT

The use of suspended ceiling tile systems has become popular in modern construction; however, fire performance data for these systems has not followed this trend. There currently is a lack of credible fire performance test data for non-rated ceiling tile systems (NCTS). This study seeks to explore failure criteria for NCTS, and thermal resistance provided prior to failure.

As part of this research, a testing apparatus was constructed to evaluate the performance of the NCTS with respect to the fire location, distance between the NCTS and a fire, and tile arrangements within the NCTS. Testing results were then compared against numerical model predictions of the observed temperatures.

The results demonstrated that the NCTS provides a measurable level of thermal resistance during a fire and maintains its integrity for several minutes. Furthermore, it was shown that testing results can be generally represented using the numerical model.

LIST OF ABBREVIATIONS USED

AHJ	Authority Having Jurisdiction
CDPT	Copper Disk Plate Thermometer
d	Distance of Thermocouple above/below Ceiling Tile [m]
D	Burner Diameter [m]
FDS	Fire Dynamics Simulator
FGS	Faculty of Graduate Studies, Dalhousie University
ΔH	Lower Heating Value [kJ kg^{-1}]
H	Height of Ceiling above Burner [m]
HRR	Heat Release Rate [kW]
k	Thermal Conductivity [kW K^{-1} m^{-1}]
l	Flame Height [m]
L	Thickness of Material [m]
LHV	Lower Heating Value [MJ kg^{-1}]
$\dot{m}$	Mass Flow Rate [kg s^{-1}]
NBCC	National Building Code of Canada
NCTS	Non-Rated Ceiling Tile System
NIST	National Institute of Standards and Technology
PT	Plate Thermometer
$\dot{Q}$	Heat Release Rate [kW]
$\dot{q}''$	Heat Flux [kW m^{-2}]
r	Radial Distance from Centreline of Plume [m]
RCTS	Rated Ceiling Tile System
SFPE	Society of Fire Protection Engineers
SLPM	Standard Litres Per Minute
ΔT	Temperature Difference Across material [°C]
T_{max}	Ceiling Temperature at a Given Point [°C]
T_∞	Ambient Temperature [°C]
ULC	Underwriters Laboratory of Canada

ACKNOWLEDGEMENTS

This research was conducted within the Fire and Explosion Laboratory in the Chemical Engineering Department of Dalhousie University. It was performed for RJ Bartlett Fire Protection Engineering under the supervision of Dr. Michael Pegg PhD, P.Eng., with assistance from Dr. Jan Haelssig PhD, P.Eng., Monica Diab, Ike Bello, and Aaron Yip. Funding for this project was provided by an NSERC Engage Grant, with technical expertise and supervision contributed in-kind from both Angela Rogers, M.Sc.E., P.Eng., and Christian Oickle, M.E., P.Eng. of RJ Bartlett Engineering Ltd.

CHAPTER 1 INTRODUCTION

1.1 MOTIVATION

Suspended ceiling tiles have been used in both commercial and residential buildings for several decades. They are attractive for construction purposes as they provide acoustic damping between building floors, provide a concealed space within which to house building services, and can be easily installed or replaced. With their rise in popularity, companies are beginning to seek the fire performance data of these suspended ceiling tile systems. While their use has become ever more prevalent, fire performance data for these systems has not followed the same trend. Currently, there appears to be a lack of fire performance test data for non-rated ceiling tile systems (NCTS).

1.2 OBJECTIVES

The primary objective of this research is to determine a criterion for the failure of NCTS assemblies. In addition to failure criteria, this research also examines the thermal resistance provided by the suspended ceiling tile system to the ceiling space above during a fire scenario, prior to failure. This is an area of interest as it may affect the fire-resistance rating attributed to the ceiling assembly, or the time to detection of a fire scenario in cases where a sprinkler or other fire detection device is situated above the ceiling tiles.

1.3 SCOPE OF RESEARCH

This section explores the scope of the research conducted. Failure of the suspended ceiling tile system has been defined as the point where flame breakthrough into the ceiling cavity above is observed. Both the failure and thermal resistance of the suspended ceiling tile

system were evaluated with respect to the location of the fire below the suspended ceiling tile system, the distance between the ceiling tiles and the point of origin of the fire, and the arrangement of the ceiling tiles within the suspended ceiling tile system. The experimental results were then compared against numerical model predictions.

1.4 Summary of Chapters

Chapter 1 introduces the research, outlining the motivation, objectives, and scope of the project. Chapter 2 provides further context to the research and insight into the application of findings. This is achieved by explaining the differences between rated and non-rated ceiling tile systems (NCTS), compliance with national and international building codes, and discussing the use of Fire Dynamics Simulator (FDS) to achieve compliance with building codes.

A review of associated literature is presented in Chapter 3, which also serves to emphasize the current lack of specific fire performance data for suspended ceiling tile systems. Where specific research related to the topic was not available, sources have been identified providing valuable insight into heat transfer to ceilings, methods for apparatus design, and heat release rates.

The testing apparatus is discussed in Chapter 4, including an overview of testing demands for the apparatus and a summary of the apparatus design and construction. Chapter 5 introduces the experimental setup and parameters such as ceiling tile layouts and type, location of the heat source, and methods for measuring and recording temperature. Chapter 6 then presents the design of experiments and sequence of testing.

Chapter 7 presents the experimental results and provides a complete analysis of the results and observed trends. This chapter explores time to failure, mode of failure, endpoint surface temperatures, failure temperatures, and gas temperatures above and below the suspended ceiling tile system. These experimental results are compared to numerical model predictions in Chapter 8. Finally, Chapter 9 summarizes the findings and presents conclusions and recommendations, drawing on the experimental results and numerical model predictions.

CHAPTER 2 BACKGROUND

2.1 RATED AND NON-RATED CEILING TILE SYSTEMS

Suspended ceiling tile systems are a critical aspect in the interior design for many modern buildings and are used across the globe in both residential and commercial applications. They allow building services to be concealed above the ceiling tile assembly, providing an aesthetically pleasing finish, while maintaining ease of access to these services. Although these systems are suspended from the ceiling assembly above them, they are not structurally considered part of the ceiling assembly.

Although suspended ceiling tile systems are not considered as a structural component of ceiling assemblies, they may be used to provide acoustic dampening between floors (sound transmission class-rating) or to provide a level of fire protection. Certain occupancies within buildings may even mandate that individual ceiling tiles carry an associated flammability and/or flame spread rating as outlined, for example, by the National Building Code of Canada [1]. In this work, suspended ceiling tile systems were classified as two types: (i) rated, and (ii) non-rated ceiling tile systems. The differences between these systems are discussed in the following paragraphs.

Rated ceiling tile systems (RCTS) are considered to include any ceiling tile system wherein individual components, including the tiles and/or framing elements, have been subjected to specific fire-performance testing such as ASTM E119 [2] to determine material fire-performance characteristics such as flame spread, smoke developed classification, and fire-resistance rating. Many RCTSs can be used as a component considered to contribute to the associated fire-resistance rating of a listed ceiling/floor assembly. Listed assemblies are

those that have been tested and listed for use by an accredited third-party testing agency such as Underwriters Laboratory of Canada (ULC), Warnock Hersey, or Intertek Canada. Conversely, non-rated ceiling tile systems (NCTS) are those that have not been tested to determine fire-performance characteristics, or in which the fire-performance characteristics do not exceed those of typical interior finishes.

There are several differences that set rated and non-rated systems apart. RCTSs typically use a denser tile material, carry an increased flame-spread rating compared to other typical interior finishes, and as already noted can be used as a component in certain fire-rated floor assemblies. The increased level of fire protection also comes with an increase in maintenance and installation measures associated with the system. These include measures to protect all fixtures, protection of all penetrations through ceiling tile membrane, the system being dependent on the use of rated tiles, and clips attached to the framing elements which are required to hold down tiles in the event of a fire scenario. NCTSs typically use a lighter material, have a flame-spread rating similar to interior finishes, and have minimal maintenance associated with system when compared to a RCTS. Further to the differences noted, the upfront costs of RCTSs are typically more than NCTSs, with the life-cycle maintenance costs of these systems also exceeding those of NCTSs.

Where the fire performance characteristics of NCTS can be quantified, their use may be shown to contribute to the fire-resistance rating of a ceiling assembly or to provide a thermal barrier to any exposed structural members above. This can be achieved by limiting observed temperatures above the ceiling tile system and increasing the “time rating” associated with an assembly, all without incurring the additional costs and maintenance

associated with a rated system. This forms the basis for the application of results obtained from this research.

2.2 Compliance with Building Codes

Codes and standards have long been an important, yet often forgotten, part of our day-to-day lives. Many help to improve the human experience by ensuring the safety of the devices, equipment, and structures we interact with every day. Building codes, for example, have been developed and used throughout modern civilizations in various forms and capacities. Historical building codes were often created or built-upon after significant fires such as the Great Fire of London in 1666, after which the Rebuilding of London Act 1666 [3] prescribed measures to limit fire spread from building to building in a dense city. These early codes formed the basis for the modern building codes currently being used.

The International Building Code [4], Life Safety Code [5] (also known as NFPA 101), and National Building Code of Canada (NBCC) [1] are examples of modern building codes, all of which are classified as model codes. Model codes are typically created by a governing body, such as an international or federal agency, and then legislated into act by individual Authorities Having Jurisdiction (AHJ), such as a state/provincial or municipal government. Model codes usually fall into two categories: either an objective-based code, or a performance-based code. Objective-based codes are those that provide a strict, prescriptive solution to designing a building while performance-based codes allow for a designer to demonstrate that a proposed design will maintain or provide an acceptable level of safety.

The NBCC [1] is a model code published by the National Research Council of Canada which functions as both an objective- and performance-based code. While this is a

nationally recognized design guideline, each province within Canada is responsible for adopting or amending it as they see fit. Depending on the province, some of these have adopted the NBCC as is, adopted the NBCC with modifications, or used the NBCC as a basis for the development of a province-specific building code. The NBCC outlines requirements for many aspects of building design including structural loading, active and passive means of fire protection, occupant safety and accessibility, and ventilation. For example, the NBCC often requires that the floor assembly of a building be constructed as a fire separation having a specific fire-resistance rating depending on the size of the building.

As previously mentioned, the NBCC functions as both an objective- and performance-based code. Division A, Sentence 1.2 of the NBCC provides requirements for compliance, stating that compliance is to be achieved by either meeting the prescriptively acceptable solutions (objective-based approach) or through the development of an alternative solution (performance-based approach). In keeping with the example presented above, the acceptable solutions presented in the NBCC do not prescriptively permit NCTSs to be considered to contribute to the associated fire-resistance rating of a floor assembly. This aside, if the fire performance of NCTSs can be quantified, the use of such systems to contribute to the fire-resistance rating of a floor assembly could potentially be rationalized through the development of an alternative solution.

When achieving compliance with the NBCC through the development of an alternative solution, the NBCC requires that a proposed assembly be shown to provide an equivalent level of protection with regards to fire and life safety as that intended by the acceptable solutions of the NBCC. Alternative solutions are typically required to be prepared by either

a licensed Architect or Professional Engineer, who then takes personal responsibility for demonstrating that an agreed-upon performance criteria has been met.

Performance criteria are intended to establish a level of acceptable risk based on the corresponding functional, objective, and intent statements associated with the prescriptive requirements of the NBCC. As outlined within the Society of Fire Protection Engineers (SFPE) Guide to Performance-Based Fire Safety Design [6], performance criteria are often established by concerns brought forward by the building designer or an AHJ, with all parties involved then agreeing to defined performance criteria that must be met. As part of demonstrating that performance criteria have been met, a proposed condition can be evaluated through an engineering analysis which may involve the use of computer-based simulation software, empirical calculations, referenced literature, and good engineering practice.

Looking once again at example of the fire-resistance rating of a floor assembly, an objective-based approach may mandate a "time rating" for the floor assembly while a performance-based approach would require that the intent of the prescriptive requirement (i.e., limiting the chance that a floor assembly exposed to fire will fail prior to occupant evacuation) be met. Therefore, if the fire performance characteristics of an NCTS are known, the system could potentially be incorporated into an empirical or numerical model used to demonstrate that a proposed condition achieves the defined performance criteria as part of the development of an alternative solution.

2.3 FIRE DYNAMICS SIMULATOR

The advent of modern computers has enabled the modelling and simulation of fire scenarios. Examples of parameters that are relevant for fire scenarios include the following:

- Fire growth and development.
- Heat and mass transfer from fires.
- Convective and forced flows from the resulting plume.
- Compartment temperatures in the fire area.

Fire Dynamics Simulator (FDS) is an open-source, Fortran-based computational fluid dynamics software used for modelling fires. FDS [7] is published by the National Institute of Standards and Technology (NIST), and as noted in the FDS Technical Reference Guide [9], was developed through an international partnership of private and public organizations.

The FDS Technical Reference Guide [8] outlines the underlying theory behind the operation of FDS. From this guide, it is noted that models are solved numerically using a large-eddy simulation version of the Navier-Stokes equation. This version of the Navier-Stokes equation is intended for low-speed thermally-driven flow, with a focus on transport of smoke and heat from fires [8]. To create a model using FDS, the user must specify properties including but not limited to the following:

- Compartment geometry and bounds of the simulated space.
- Properties of materials within the simulated space.
- Design fire size and location.

- Characteristics of combustion such as fuel loads, heat release rates, and combustion by-products.
- Grid/mesh sizes within the simulated space.
- Desired outputs from the model.

Desired outputs from the model are exported to a data file which can then be used with a program such as Smokeview (a companion program to FDS) for visualisation or Microsoft Excel for data analysis. A sample visualization of an FDS model output using Smokeview is provided in Figure 1. This FDS model was created by RJ Bartlett Engineering as part of the development of a report which used FDS to represent possible worst-case scenario fires within a four-storey residential townhouse building.

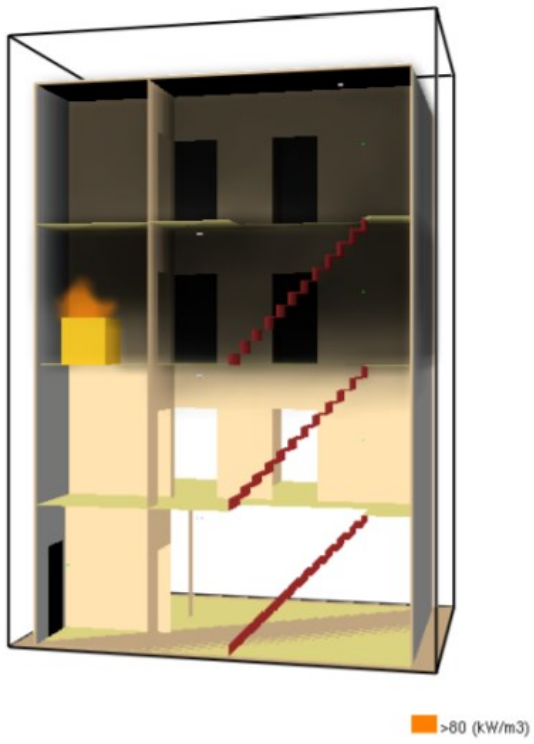

Figure 1 Sample visualization of FDS model. Courtesy of RJ Bartlett Engineering Ltd Report "12070 Final FPE Analysis R140327" [9]

The Fire Dynamics Simulator User's Guide [10] states that the program is primarily used for two purposes related to studying fire dynamics and solving fire protection engineering problems. About half of the program's uses are attributed to the design of smoke handling systems and sprinkler/detector activation studies, while the other half of uses are for the recreation of residential or industrial fires. In addition to the uses noted above, FDS can be used for the development of alternative solutions. FDS may be used in this way to determine expected conditions from a worst-case fire scenario such as incident heat flux received by an object, smoke obscurity *vs*. time, sprinkler activation times, or exposure temperatures. These expected conditions can then be evaluated against proposed building conditions, with the end goal being to demonstrate that the proposed condition will be acceptable.

Where installed within a building, suspended ceiling tile systems can influence sprinkler activation times as sprinklers are often required to be installed at the level of the system. With the relatively low exposure temperatures required for sprinkler activation (typically between 57 °C and 77 °C) it is conservative to assume that a NCTS would stay intact during the time required to achieve sprinkler activation. However, since sprinkler systems are only considered to suppress and not extinguish a fire, and the fire performance characteristics of NCTSs have not been quantified, it is unknown how long the integrity of the tiles would be maintained in a fire scenario. If these characteristics can be quantified, NCTSs could be potentially included within an FDS model after sprinkler activation.

In the development of an alternative solution utilizing FDS to form the basis of a technical rationale, if the fire performance of NCTSs can be quantified they could be included within the model and used to provide a thermal barrier to the space above, reducing estimated

exposure temperatures to the above assembly and potentially increasing the associated time rating. The experimental findings of this research have been compared to a similar FDS model in Section 8 to determine how well these results can be replicated numerically within FDS.

CHAPTER 3 LITERATURE REVIEW

Several topics were identified early in the process of conducting the literature review that provided insight into the focus of, and how the research should be conducted. This research looks specifically at the fire performance properties of suspended ceiling tile systems, heat transfer from flames, heat transfer to ceiling assemblies, methods and means of measuring and calculating heat release rate, temperature distributions across ceiling assemblies, and heat transfer through solids. Various literature on these topics has been identified in a wide variety of formats ranging from peer-reviewed journal articles to published industry standard test methods.

Literature was available regarding heat transfer to ceilings from various flame types (i.e., buoyant plume, diffusion flame, impinging jet, etc.), several models for determining temperature profiles along the ceiling above a fire based on heat source, size, and distance from ceiling, and methods for measuring temperature and incoming heat flux (e.g., plate thermometers, heat flux sensors, thermocouples, and copper disk plate thermometers (CDPT)). It is noted that from the literature reviewed that most research and methods are aimed towards an unconfined ceiling while this research pertains to fires within a room (i.e., a contained fire).

3.1 Fire Performance of Suspended Ceiling Tile Systems

Many manufactures of ceiling tiles provide several different products, some simply providing an acoustic barrier, and others offered as a “fire-rated” product. To achieve these ratings, the tiles are subjected to tests such as ASTM E84 “Standard Test Method for Surface Burning Characteristics of Building Materials” [11] and ASTM E119 “Standard

Test Methods for Fire Tests of Building Construction and Materials" [2]. These tests are conducted solely on a sample of the ceiling tile materials, and not upon the entire suspended ceiling tile system.

As the testing procedures outlined within ASTM E84 and ASTM E119 are completed on only a sample of the material, these tests would not necessarily be representative of how an entire suspended ceiling tile system will perform in a fire scenario. Furthermore, these tests do not provide specific insight into the mode of failure of a suspended ceiling tile system or their overall performance during a fire scenario.

A review of literature regarding the fire performance of entire suspended ceiling tile systems yielded almost no results, indicating that this may be a field lacking adequate public research. Brannigan [12] notes that many "fire-rated" ceiling tiles are simply tested to ASTM E84 and as such have an associated flame spread rating but do not provide any fire-resistance. In addition to this, Brannigan [12] notes that the test standards themselves, specifically ASTM E119, do not take into consideration "real-life circumstances" with regards to the real-life application of the determined fire resistance ratings. Furthermore, he also discusses the hazards posed to firefighters from the failure of these suspended ceiling tile systems and the chances of entanglement from their collapse.

3.2 HEAT TRANSFER

When conducting fire research, proper quantification of the fire is one of the most important steps to be made. Babrauskas proposes the notion that the HRR of a fire is "the single most important variable in determining fire hazard" [13]. He notes that while deaths in fires are typically attributed to the formation of toxic gases, the heat release rate of a fire

provides the greatest insight into the hazard posed specifically by the fire. Where the heat release rate of the fire is known, the fire can be effectively quantified with regards to flame height, heat transfer rate to other objects, and temperature profiles surrounding the fire itself. Therefore, it is important to review the methods by which the HRR is determined and measured.

The HRR of a fire can be determined through several different means. ASTM E906 [14] provides a standard method for measuring the heat release rate for unknown combustibles, while measurement of oxygen consumption and species production can also provide a means of calculating the HRR through the use of an oxygen depletion calorimeter [15] or cone calorimeter [16]. In addition, where the combustion properties or burning characteristics of a fuel are known, the HRR can be determined through measurement of mass loss or mass flow rate of the fuel.

Various research has been conducted studying heat transfer from flames to a ceiling. Baukal and Gebhart [17] studied heat transfer from natural gas flames to a ceiling through the use of a water cooled disk, with the focus of the research being specifically on the impact of surface effects and the rate of heat transfer to the ceiling itself as opposed to the observed temperature profiles. Similar research has been completed such as that by Hu et. Al [18] and Li et. Al [19] who have completed research regarding heat transfer from flames to a ceiling and associated temperature profiles, however both of these studies have incorporated either longitudinal forced flows and/or ceiling extraction as these research topics were aimed towards ceiling jet flows in corridors and channel ceilings.

In addition to heat transfer from flames to ceilings, various research has been completed studying heat transfer from flames to other objects for industrial applications such as that of Remie et. Al [20] however in this and other cases, the study focused specially on heat transfer from a laminar jet flame. Chander and Ray [21] present a review of research that has been completed regarding flame impingement heat transfer in which it is noted that all referenced models and research completed specifically studied heat transfer from either a single- or multiple-jet flame source.

In a real-life fire scenario, the flame pattern of a fire follows that of a natural diffusion flame (except where the flame may be affected by the air flow pattern within the compartment, i.e., jet flow or fire whirl). Various research has been completed in this area, such as that by Ding and Quintiere [22] which studied the radial length of a flame under a ceiling, air entrainment, and flame profiles and aimed to develop an integral model for turbulent flame radial lengths. Kokkala [23] studied heat transfer to a ceiling from an impinging diffusion flame and found the observed gas temperatures and heat transferred to the ceiling to be functions of the ratio of the ceiling height and flame height. Drysdale [24] proposes the following correlation for the flame height of a buoyant diffusion flame in which $\dot{Q}$ is the heat release rate [kW], l is the apparent flame height [m], and D is the burner diameter [m]:

$$l = 0.23\dot{Q}^{0.4} - 1.02D \tag{1}$$

which is valid where

$$7 < \dot{Q}^{0.4}/D < 700 \tag{2}$$

The temperature profile across the ceiling during a fire must be known to accurately determine the temperatures observed at the time of ceiling failure. Alpert [25] presents two correlations (using imperial units) for the gas temperature distribution across a ceiling based on the radial distance from the centerline of the fire; this model is also accepted and used by Drysdale [24]. The two correlations, as presented by Drysdale (using metric units) are as follows:

$$T_{max} - T_{\infty} = \frac{5.38(\dot{Q}/r)^{2/3}}{H} \qquad r > 0.18H \qquad (3)$$

and

$$T_{max} - T_{\infty} = \frac{16.9\dot{Q}^{2/3}}{H^{5/3}} \qquad r \leq 0.18H \qquad (4)$$

where T_{max} is the ceiling temperature at a given radius [°C], T_{∞} is the ambient temperature [°C], H is the ceiling height [m], and r is the radial distance from centerline of fire plume [m].

Regarding fires located near a wall or corner, Drysdale [24] states that temperatures will be higher due to a combination of air being entrained into the plume at a lower rate and the ceiling flow no longer being symmetric. To account for this, $\dot{Q}$ should be multiplied by a factor of two where the fire is located near a wall and a factor of four for corners. This correlation begins to break down for values of l/H greater than 2, as the portion of the flame deflected horizontally begins to form a portion of the ceiling jet.

With respect to heat transfer through solids, Bergman et al. [26] notes that for a one-dimensional plane wall at steady state, heat flux can be calculated as follows:

$$\dot{q}'' = k\frac{\Delta T}{L} \qquad r > 0.18H \qquad (5)$$

where $\dot{q}''$ is the heat flux [kW m^{-2}], k is the thermal conductivity of the material [kW $K^{-1}m^{-1}$], ΔT is the temperature difference across the material [°C or K], and L is the thickness of the material [m].

From Equation 5, it is apparent that where the temperature difference across a plane wall is known (or measured), in conjunction with knowing the thickness of the wall, L, and k of the material, the $\dot{q}''$ (or the heat transfer rate through the material) can be estimated.

3.3 METHODS

The general design of the apparatus followed the design described by Kokkala [23] for studying heat transfer to a ceiling from an impinging diffusion flame. A schematic drawing of this apparatus, as taken from Kokkala [23], is presented in Figure 2.

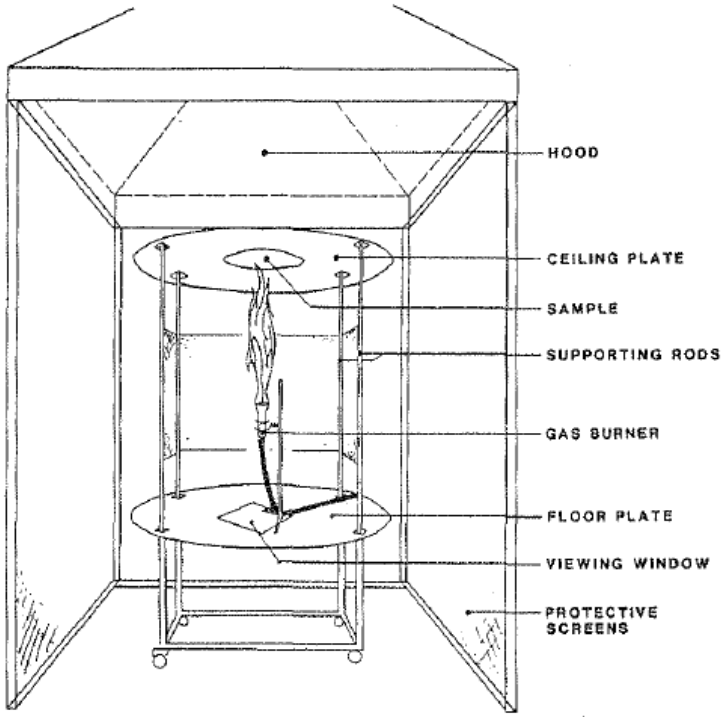

Figure 2 "*Figure 1. Schematic picture of the experimental system*" as presented in Kokkala's Experimental Study of Heat Transfer to Ceiling from an Impinging Diffusion Flame [23].

A propane burner was the primary heat source used during these experiments, creating a buoyant diffusion flame. Propane has a lower heating value (LHV) of 46.4 MJ kg^{-1} [27]. Based upon the LHV, the HRR of the fire can be determined by measuring the mass flow rate of propane to the burner. The heat release rate can be calculated as follows:

$$\dot{Q} = \dot{m}\Delta H \tag{5}$$

in which $\dot{m}$ is the mass flow rate [kg s^{-1}] and ΔH is the LHV of propane [MJ kg^{-1}].

To measure the incident heat flux received by the suspended ceiling tile system, the surface temperature of the ceiling must be known. As there is a larger incident heat flux and higher temperatures below the ceiling tiles, traditional surface thermocouples cannot be

employed. As an alternative, the use of plate thermometers (PT) was considered. This would allow not only for a more accurate measurement of the ceiling tile surface temperature, but also for the calculation of incident heat flux using the adiabatic surface temperature (AST) as shown by Wickstrom [28].

While the use of a plate thermometer would prove a useful tool, both Wickstrom [28] and Robbins [29] found plate thermometers to have a slow response time, and they are therefore unreliable for capturing rapidly changing temperatures. To speed up the response time, Wickstrom [30] proposed the use of a modified PT; the copper disc plate thermometer (CDPT). These are made of a thermocouple bonded to the back of a pure copper disk, 12 mm in diameter, 0.2 mm thick. This is then backed with insulation and mounted into a hole in the sample specimen, flush with the surface. Although this no longer allows for calculation of incident heat flux using the AST, it does provide a more accurate surface measurement of transient surface temperature variations with a faster response time than that of a traditional PT (which may take upwards of 400 s to reach a steady state response as shown by Robbins [29]).

CHAPTER 4 APPARATUS DESIGN

To perform this research, an apparatus was required to be designed and constructed capable of meeting the following requirements:

1. The apparatus was to be capable of holding arrangements of both two 610 mm × 1 220 mm ceiling tiles and four 610 mm × 610 mm ceiling tiles.
2. A closed cavity (approximately 610 mm high) was to be provided above the ceiling tiles, representative of a typical commercial installation.
3. The apparatus was to permit heat transfer to the ceiling tiles through the use of open flames from a variable location.
4. The distance between heat source and the ceiling tiles was to be capable of being adjusted between 250–500 mm.
5. A means to measure and record HRR, temperature, and flame breakthrough into the cavity above was to be provided.

The general concept for the apparatus design was taken from that used by Kokkala for studying heat transfer to a ceiling from an impinging diffusion flame [23]**.** Modifications were made to this design to ensure that the above noted requirements could be met. A conceptual image of the apparatus is shown in Figure 3.

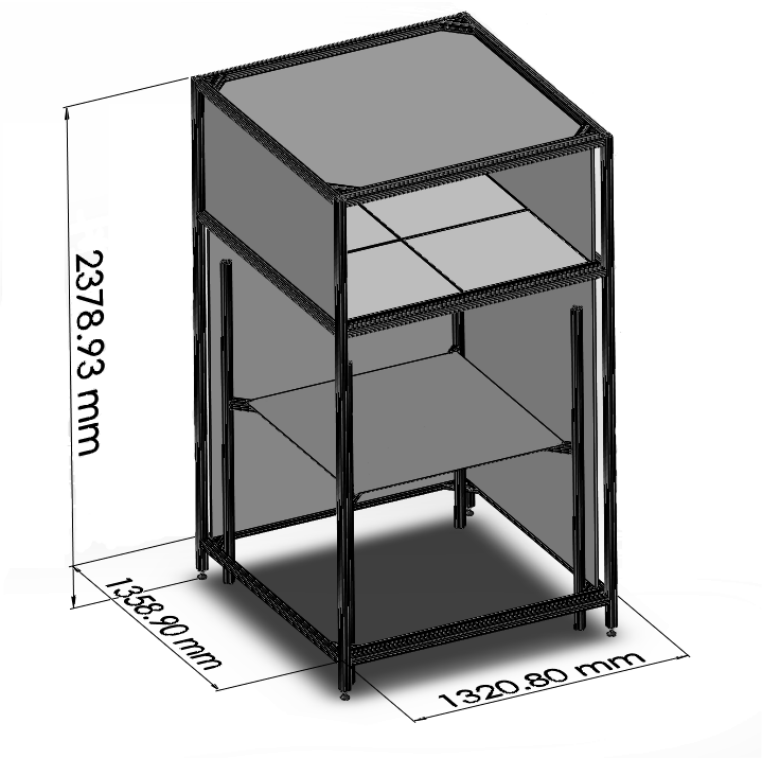

Figure 3 Conceptual image of the testing apparatus.

An image of the actual test apparatus is provided in Figure 4, which also identifies individual components and systems of the apparatus. A description of these components and systems is provided in the following sections.

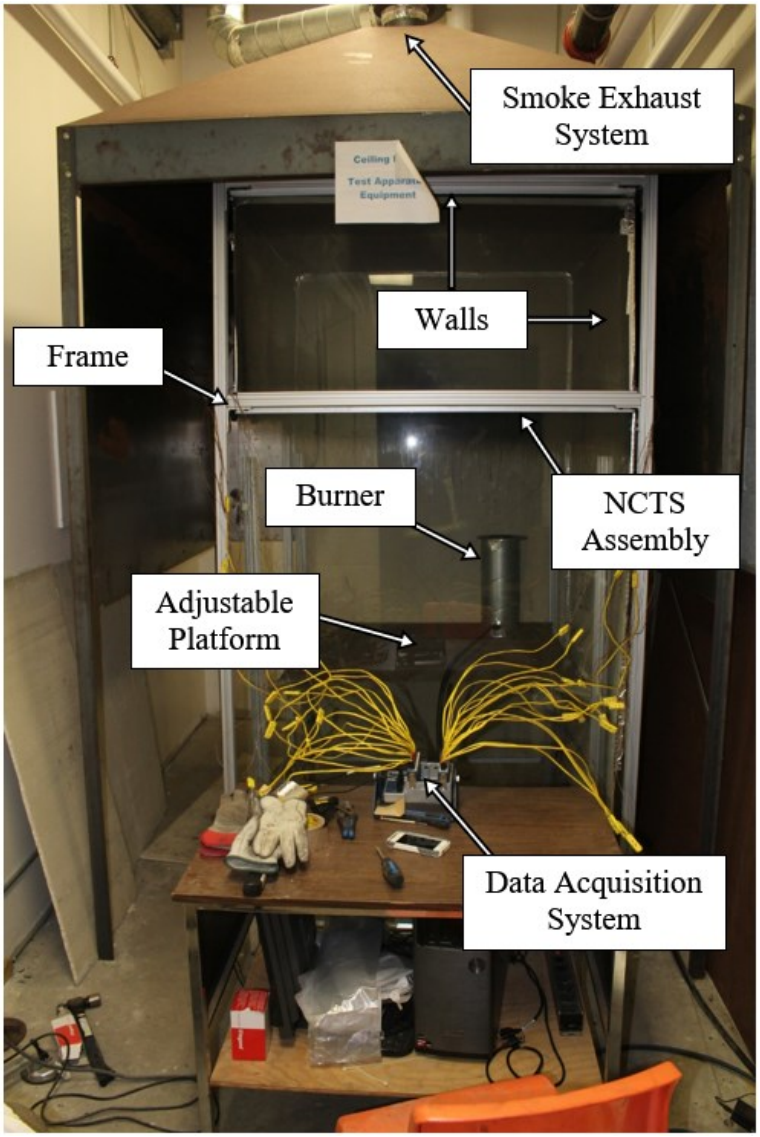

Figure 4 Image of the testing apparatus identifying individual components and systems.

4.1 Apparatus Frame

The frame for the apparatus was made from square aluminum T-slotted framing. T-slotted framing is modular and easy to assemble because all joints are held together with brackets and bolts, thus allowing for the apparatus to be easily reconfigured. The apparatus had a footprint of approximately 1 320 mm × 1 360 mm, with an overall height of approximately 2 380 mm. This height provided adequate space for a cavity above the tiles as well as sufficient working space below the tiles for the height of the heat source to be adjusted. An image of the apparatus frame and cavity space is provided in Figure 5.

Figure 5 Testing apparatus frame and cavity space.

4.2 Apparatus Walls

The apparatus had two full length walls made of fiberglass reinforced cement board at the rear and right-hand side, with a fourth front wall made of tempered glass to allow for viewing and monitoring of experiments (both above and below the ceiling tile system). The distance between the walls was 1 220 mm × 1 220 mm, allowing enough space for the

ceiling tile array and framework. The left-hand side wall of the apparatus was also made of fiberglass reinforced cement board and open below the ceiling tiles, only covering the cavity above the tile assembly, to allow an exit for smoke from the apparatus. Cement board was chosen as a material for the walls of the apparatus due to its relatively low thermal conductivity, fire resistance, and similarity to drywall materials used in building construction. An image of the apparatus walls is provided in Figure 6.

Figure 6 Cement board walls of the apparatus, as viewed from the interior.

4.3 Adjustable Platform

A platform was installed inside of the apparatus below the ceiling tile assembly. This platform allowed the distance between the platform surface and the ceiling tiles to be adjusted from 150–1 830 mm. The platform consisted of four main pillars connected by cross members (all constructed using aluminum T-slotted framing) with a 1 020 mm square sheet of 3.18 mm thick steel resting across the top as a working surface. This steel plate was selected to provide a sturdy flat surface while permitting the use of various heat sources

such as a gas burner, wood cribs, or an electrical heating element. The adjustable platform frame and surface is shown in Figure 7.

Figure 7 Adjustable platform surface and heat source within the apparatus.

4.4 Smoke Exhaust System

The apparatus was contained below an 1 830 mm square extraction hood to assist in removing smoke from the testing area. Skirts made of 1.02 mm sheet steel extended down from the hood a distance of 1 220 mm on three sides to assist in the entrainment of air into the exhaust ducting. The venting of exhaust gases was aided by a 525 m^3 h^{-1} electric blower attached to the top of the extraction hood and connected to the exhaust ducting. The exhaust system was designed to accommodate the future addition of a means for measuring heat release rate using oxygen depletion calorimetry, requiring measurement of exhaust gas composition as well as the exhaust mass flow rate. To facilitate these additions, the duct system was built based on the dimensional guidelines set out in ASTM E1354 [15]. The smoke exhaust system is shown in Figure 8.

Figure 8 Smoke exhaust system with apparatus removed except for the adjustable platform framing.

4.5 Ceiling Tile Material Properties

The ceiling tiles used as part of this testing were Armstrong® 902A MR (Mold Resistant) Acoustical Ceiling Tile Panels, reclaimed from a renovation project taking place in 2017 on the Dalhousie University Sexton Campus in Halifax, Nova Scotia. These tiles were chosen because they had been installed within a building for an extended time. Therefore, they would help to provide a more accurate representation of ceiling tiles installed in older buildings. Many of the ceiling tiles had sustained either physical damage or water damage. As such, the reclaimed tiles were sorted and those in the best condition were selected for use in tests.

Based on the manufacturer's product safety data sheet [31] for Armstrong® 902A MR Acoustical Ceiling Tile Panels, the ceiling tiles are composed of a combination of newsprint, perlite, fiberglass, ground Calcium carbonate, mineral wool, starch, kaolin clay, quartz (inbound), and antimony oxide. Select material properties of the ceiling tiles used during testing are presented in Table 1. These values have been taken from a combination of physical measurements and referenced literature.

Table 1 Material properties of Armstrong® 902A MR acoustical ceiling tile panels.

Material Property	Value
Thickness (Measured)	12.5 mm
Density (Product Data) [25]	N/A
Density (Measured)	194 ± 5 kg m^3
Thermal Conductivity [24]	0.058 W m^{-1} K^{-1}
Specific Heat [24]	1 340 J kg^{-1} K^{-1}
Decomposition Temperature [25]	1 093 °C (Perlite)

CHAPTER 5 EXPERIMENTAL SETUP

This chapter provides an overview of the experimental setup for performing tests. Included is a description of the ceiling tile arrangements, heat source, and equipment for temperature measurement.

5.1 CEILING TILE ARRAY

The ceiling tile array was positioned such that there would be a 610 mm high cavity above the tiles. The size of this cavity was intended to be representative of that which would be found in a commercial installation for building services located above the tiles. L-shaped angle molds were the main structural support for the ceiling tile array; these molds were secured with bolts passing through the cement board walls and into the apparatus frame. From the molds, T-shaped framing could be arranged to accommodate either 4-tiles or 2-tiles as shown in Figure 9. The T-shaped framing can be easily assembled and snaps into place. In this work, both 4-tile and 2-tile arrangements were tested.

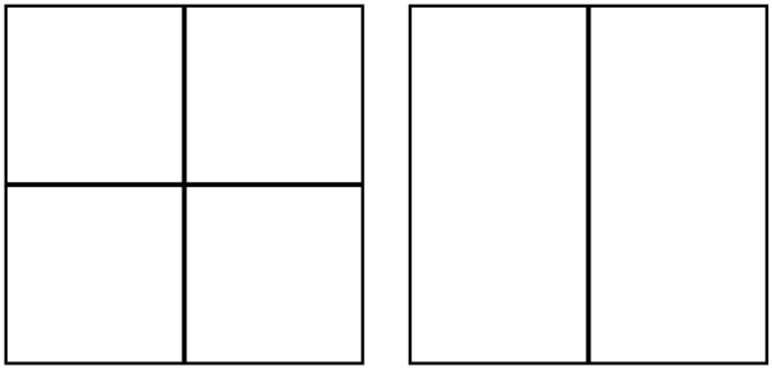

(a) (b)

Figure 9 Ceiling tile arrangements tested as part of this research, as viewed from above/below: (a) four 610 mm × 610 mm tiles; and (b) two 610 mm × 1 220 mm tiles.

An image of the installed ceiling tiles is provided in Figure 10. The cavity space above an installed four-tile arrangement is shown in Figure 11.

(a) (b)

Figure 10 Installed (a) four-tile and (b) two-tile arrangements, viewed from below.

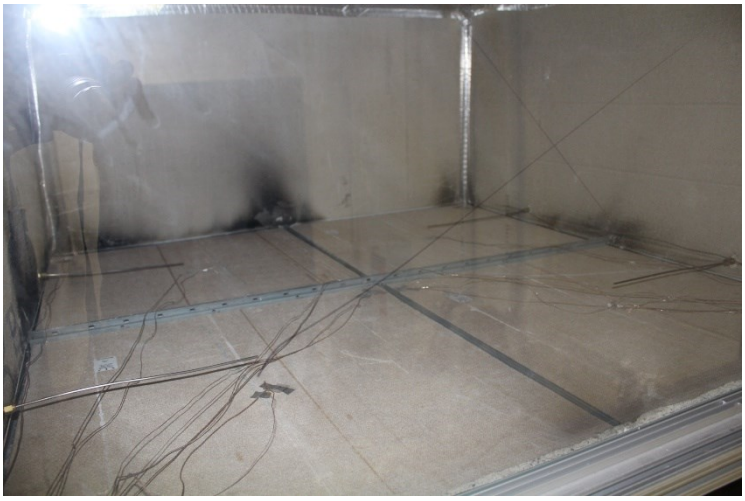

Figure 11 Cavity space above the ceiling tiles for an installed four-tile arrangement.

5.2 HEAT SOURCE

A propane burner was the primary heat source used during the experiments to create an easily controlled buoyant diffusion flame. Propane entered at the bottom of the burner, which had an inner diameter of 102 mm, passed through a layer of steel wool, and then through a packed bed of sand beads resulting in a low momentum flame.

The distance between the ceiling tiles and the propane burner, *H*, was adjusted between 250 mm and 500 mm during testing, permitting flame impingement on the ceiling to be controlled. The experimental setup of the burner is shown in Figure 12.

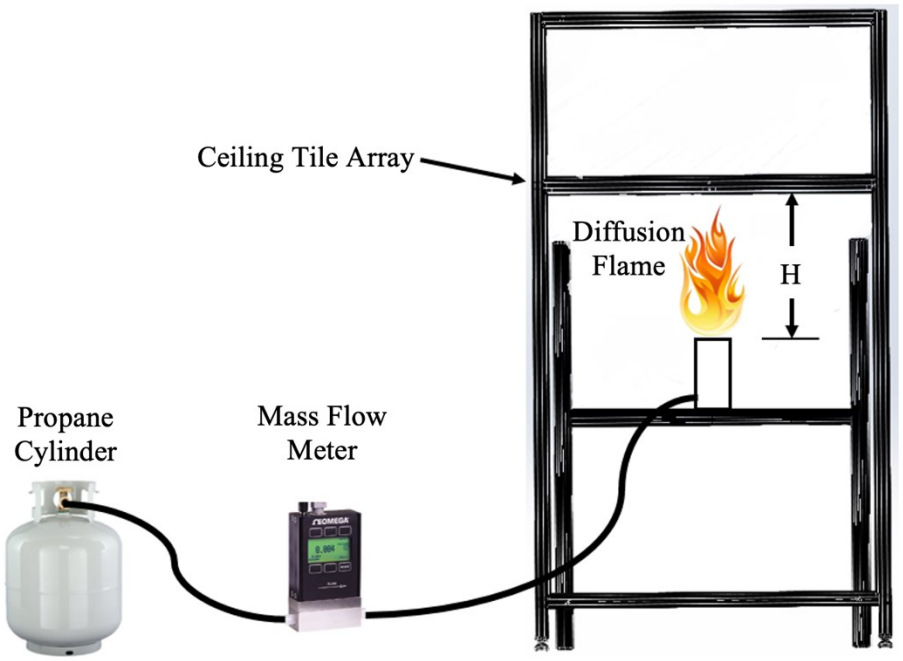

Figure 12 Schematic representation of the heat source used during experiments including fuel supply, means of measurement, and location of the burner relative to the location of the ceiling tiles array.

Propane has a lower heating value of 46 400 kJ kg^{-1} [27], equal to 1.38 kW of heat release for each standard litre of propane gas burned per minute using a density of 1.787 kg m^{-3}. The flow rate of propane into the burner was measured using a "FMA-2608A Mass and Volumetric Gas Flow controller" from Omega (as shown in Figure 12).

The accuracy of the flow rate controller was ± (0.8% of the reading + 0.2% of the full scale) the controller had a response time of 100 ms, and a maximum volumetric flow of 20 SLPM.

This allowed for a maximum heat release rate of 27.6 ± 0.276 kW while using the flow rate controller.

While the flow rate controller used in this experiment was indicated to have a maximum flow rate of 20.0 SLPM, which is equal to a HRR of 27.6 kW using propane, after conducting preliminary tests it was found that this flow rate decreased throughout the duration of a full test. After some further preliminary testing, it was found that a consistent flow rate of 10.0 SLPM, which is equal to a heat release rate of 13.8 kW using propane, could be maintained throughout the course of a test. It is noted that, while studying heat transfer to ceilings from an impinging diffusion flame on a similar scale, Kokkala [23] used heat release rates of 2.9–10 kW. Based on the similarities of this research and that of Kokkala [23], it was decided to move forward using an HRR of 13.8 kW. A sample image of the propane burner in operation is provided in Figure 13.

Figure 13 Propane burner in operation at a heat release rate of 13.5 kW with flame impingement on the ceiling tile system.

5.3 HEAT SOURCE LOCATION

Suspended ceiling tile systems are typically comprised of ceiling tiles, supporting construction (i.e., frame pieces and hangars), and openings for building services such as lighting fixtures and air diffusers. As the purpose of this research was not aimed at the failure of building services, two primary modes of failure were identified; either the ceiling tiles themselves would fail and permit the passage of flame into the cavity above or the supporting frame would fail and no longer be capable of supporting the individual tiles. To test for both modes of failure and determine which would be more likely to occur, experiments were conducted with either the heat source focused beneath the intersection of the framing elements or focused beneath the ceiling tiles themselves.

5.4 TEMPERATURE MEASUREMENT

As the focus of this research was the thermal resistance of the ceiling tile system and its temperature at failure, temperature was measured on the surface of the ceiling tiles and gas temperatures were measured near the surface (both above and below). To perform these measurements, three different types of thermocouples were used. As part of this study, temperature measurements were averaged and reported by the data acquisition system at time intervals of one second. The thermocouple types used during experiments are described in the following sections.

5.4.1 K-Type Sheathed Thermocouples

Eight K-Type exposed junction sheathed thermocouples from Omega (Model #KTSS-18E-21) were used for gas temperature measurements above and below the ceiling tiles. A

distance, *d*, of 20.0 mm was maintained between the ceiling tiles and the thermocouples. This allowed gas temperature to be measured both above and below the ceiling tiles and compared with the measured surface temperatures.

The thermocouples used were rated to a maximum of 1 250 °C and have an accuracy of ± 0.75 %. The sheaths have an outside diameter of 3.18 mm, a length of 610 mm, and a maximum rated temperature of 900 °C.

These thermocouples were used because they could resist the high temperatures inherent to fire testing. Furthermore, these thermocouples could be inserted through the walls of the apparatus, allowing the placement of the probe and distance from ceiling tile to be easily adjusted.

5.4.2 K-Type Surface Thermocouples

Twelve self-adhesive polyimide fast response surface thermocouples from Omega (Model #SA1-K) were used to measure the surface temperature above the ceiling tiles. These were selected for their ease of installation. Their maximum continuous rated working temperature is 175 °C (limited by the properties of the adhesive material) with an accuracy of ± 0.75 %.

These thermocouples have a low operational temperature limit and therefore could only be used in the cavity above the tiles where lower temperatures and no direct flame exposure before ceiling failure were expected. As the operational temperature limit of the surface thermocouples was limited by the ability of the adhesive material to maintain its bond, foil

tape was used to hold the thermocouples in place at higher temperatures. This proved to be an effective means of increasing the operational temperature limit.

5.4.3 Copper Plate Disk Thermometers

Following the methods proposed by Wickstrom [30], twelve copper disk plate thermometers (CDPT) were constructed and used to measure the surface temperature below the ceiling tiles. These CDPTs were constructed with 0.25 mm K-Type thermocouples (having an accuracy of 0.75 %) bonded to the copper discs. Several means to bond the thermocouples to the copper discs were attempted (including soldering and spot welding); however, it was found that silver solder was the most effective means to achieve this.

The maximum operational temperature of these thermocouples was limited by the melting point of copper, which is approximately 1 080 °C. The thermocouples were installed as discussed in Section 3.3 of this report. However, as the ceiling tiles were found to have a thermal conductivity comparable with insulation materials, the CDPT was mounted directly to the surface of the tile, with the thermocouple leads passing through the tile. The installation of the CDPT is shown in Figure 14.

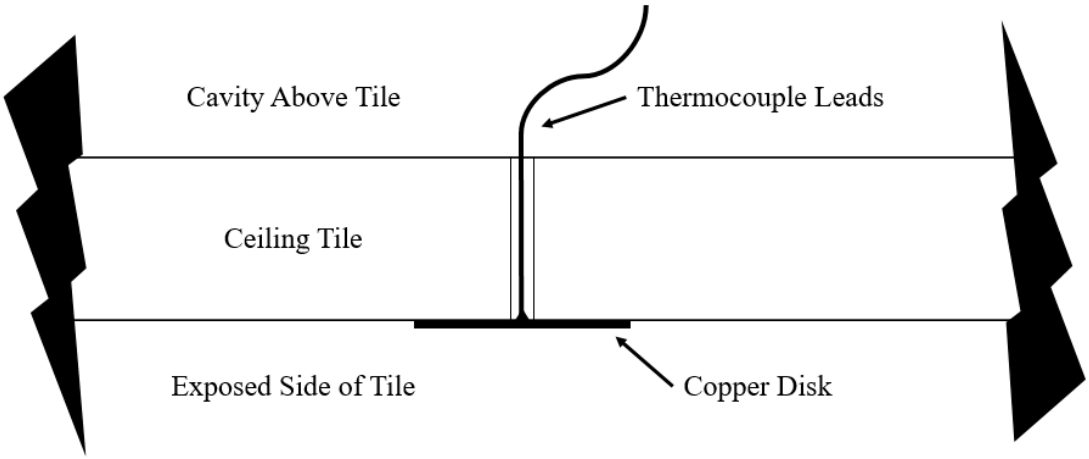

Figure 14 Cross-sectional view of a ceiling tile showing the installation of a copper disk plate thermometer.

5.4.4 Location of Thermocouples

Surface temperatures were measured using thermocouples located above and below on the center-of-the-apparatus, as well as the corner, middle, and far side corner of each tile. Gas temperatures were measured above and below the center of each tile at a distance, *d*. The thermocouples used to measure surface temperature were located directly above one another, allowing for calculation of heat transfer rates through the tiles at each location. The thermocouple arrangement for each tile is shown in Figure 15.

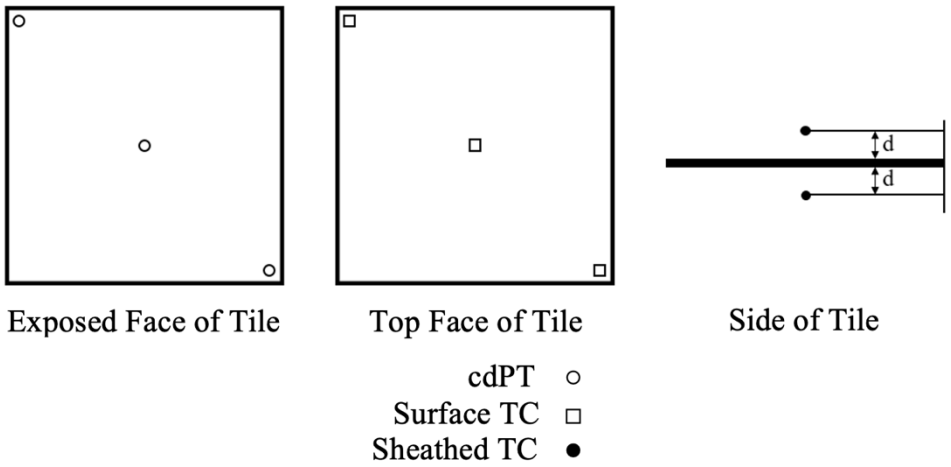

Figure 15 Type, number, and location of thermocouples used to measure temperature above and below each tile.

CHAPTER 6 EXPERIMENTAL DESIGN

This chapter provides an overview of the experimental design and includes the basis for the design of experiments, description of experimental parameters, and sequence of testing with associated parameters used for each test.

6.1 BASIS FOR EXPERIMENTAL DESIGN

Babrauskas [13] noted that heat release rate is one of the most important factors in determining the hazard posed by a fire. Kokkala [23], after conducting a series of tests on the heat transfer rate to a ceiling from an impinging diffusion flame, concluded that the total heat received by the ceiling was directly related to the observed flame height and the distance between the ceiling and the fire source. With regards to determining flame heights, Drysdale [24] presents a model which is a function of the total heat release rate of the fire and diameter of the heat source. These parameters were used to form the basis upon which the experiments were designed.

After conducting several preliminary tests, wherein a four-tile arrangement was tested using various heights of the ceiling above the burner, heat release rates, and burner locations, it became apparent that failure of the ceiling tiles themselves would likely occur prior to failure of the framing system. Based on these preliminary results, ceiling tile arrangement was also identified as a factor that could have a significant impact on failure of the ceiling tile system.

To provide a closer look specifically at failure of the individual ceiling tiles, ceiling tile arrangement, and height of the ceiling above the burner (affecting ceiling temperature and

level of flame impingement), and three heat source locations (two for the four tile-arrangement) were used as parameters in determining the failure temperature of the suspended ceiling tile system. While also considered an important parameter to explore, a constant heat release rate was used for all experiments to provide a baseline upon which the remaining factors could be compared.

In these experiments failure of the suspended ceiling tile system was defined as the point where flame breakthrough into the cavity above was observed.

6.2 Experimental Parameters

To establish a criteria for the failure of suspended ceiling tile systems, the main effect of each parameter was examined in addition to any observed interactions between these parameters. To characterize each parameter, the distance between the burner and ceiling and the tile arrangement were assigned one of two values while the burner was tested at three locations. Using these extremes allowed the observed effect of each parameter to be maximized but limited the ability to observe non-linear interactions. The experiments were conducted following a full factorial design, as full replication of these parameters would provide the best estimate of the observed variation.

Three locations for the propane burner were considered as a parameter for this study. For the purpose of tracking experimental parameters, locating the burner at the centre of the apparatus was assigned a value of “C” (centre), locating the burner below the centre of the right-hand rear ceiling tile was assigned a value of “RR” (right-rear), and for the two-tile arrangement, locating the burner below the centre of the right-hand tile was given a value of “RC” (right-centre). These burner locations are illustrated in Figure 16.

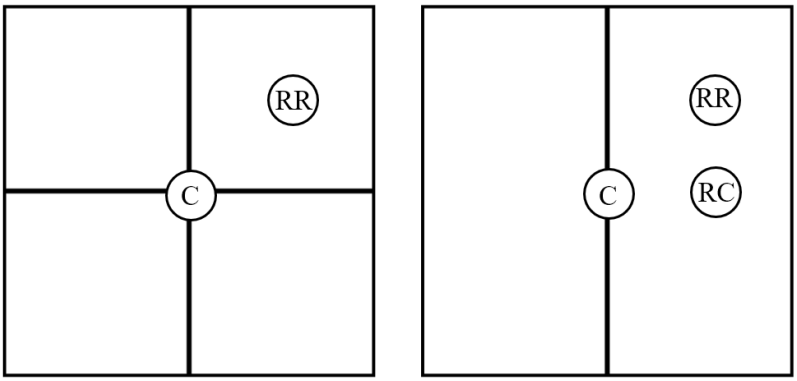

Figure 16 Burner locations used during experiments shown relative to each ceiling tile arrangement used for (a) four 610 mm x 610 mm tiles; and (b) two 610 mm x 1 220 mm tiles.

With regards to the distance between the suspended ceiling tile system and the heat source, the parameter values are limited by the physical size of the apparatus. Based on an expected flame height of 550 mm calculated using Equation 1, heights of the ceiling above the burner of 250 mm and 500 mm were selected as test parameters to provide varying levels of flame impingement on the ceiling tiles.

6.3 SEQUENCE OF TESTING

In keeping with a full factorial design of experiments, ten tests were conducted to allow each combination of the three parameters to be tested. The values of each parameter used during all experiments are outlined in Table 2 [31].

Table 2 Outline of testing sequence detailing which parameter values were used in each replicate.

Test #	Distance Between Burner and Tiles (mm)	Ceiling Tile Arrangement	Burner Location
1	500	4	RR
2	500	4	C
3	500	2	RR
4	500	2	RC
5	500	2	C
6	250	4	RR
7	250	4	C
8	250	2	RR
9	250	2	RC
10	250	2	C

CHAPTER 7 RESULTS AND ANALYSIS

7.1 OVERVIEW OF TEST RESULTS

This section provides a summary of the duration of the experiments and failure of the ceiling tile systems. Each test was run until failure occurred up to a total duration of approximately 25–30 minutes, at which point the tests were terminated regardless of whether failure was observed. A maximum time of approximately 25–30 minutes was selected as it was found that beyond this point, smoke accumulation within the apparatus hood/room began to exceed the capacity of the smoke extraction system. The following sections discuss the observed temperatures during each test, time to failure (where observed), and the condition of the ceiling tiles at the end of the test.

7.1.1 Observed Temperatures During Tests

The first step in completing an analysis of the test data was to review the temperatures observed during the tests. As previously mentioned, the tests continued until failure occurred or, where failure was not observed, up to a duration of approximately 25–30 minutes. Gas and surface temperatures were measured both on the exposed-to-fire and unexposed sides of the NCTS and provided a total of 32 sampling points during the tests (as discussed in Section 5.4.4). To assist in analyzing the resulting data against existing correlations, each sampling point and proposed burner location were assigned an XY coordinate using the right rear corner of the apparatus as a reference point such that the data could be converted to a radius-based system with respect to the burner location used in each test. To reduce the overall number of data points and allow for smoothing of the

data, samples taken at the same radius and condition (i.e., exposed/unexposed, gas/surface) were averaged for a given time step.

To provide a representative sample of the observed temperatures during each test, Figure 17 and Figure 18 present the observed temperatures at a radius near, mid distance, and far away from the burner. It is noted that the fixed nature of the sampling locations with respect to burner location (which could not be easily adjusted between tests) resulted in different sampling point radii for each burner location.

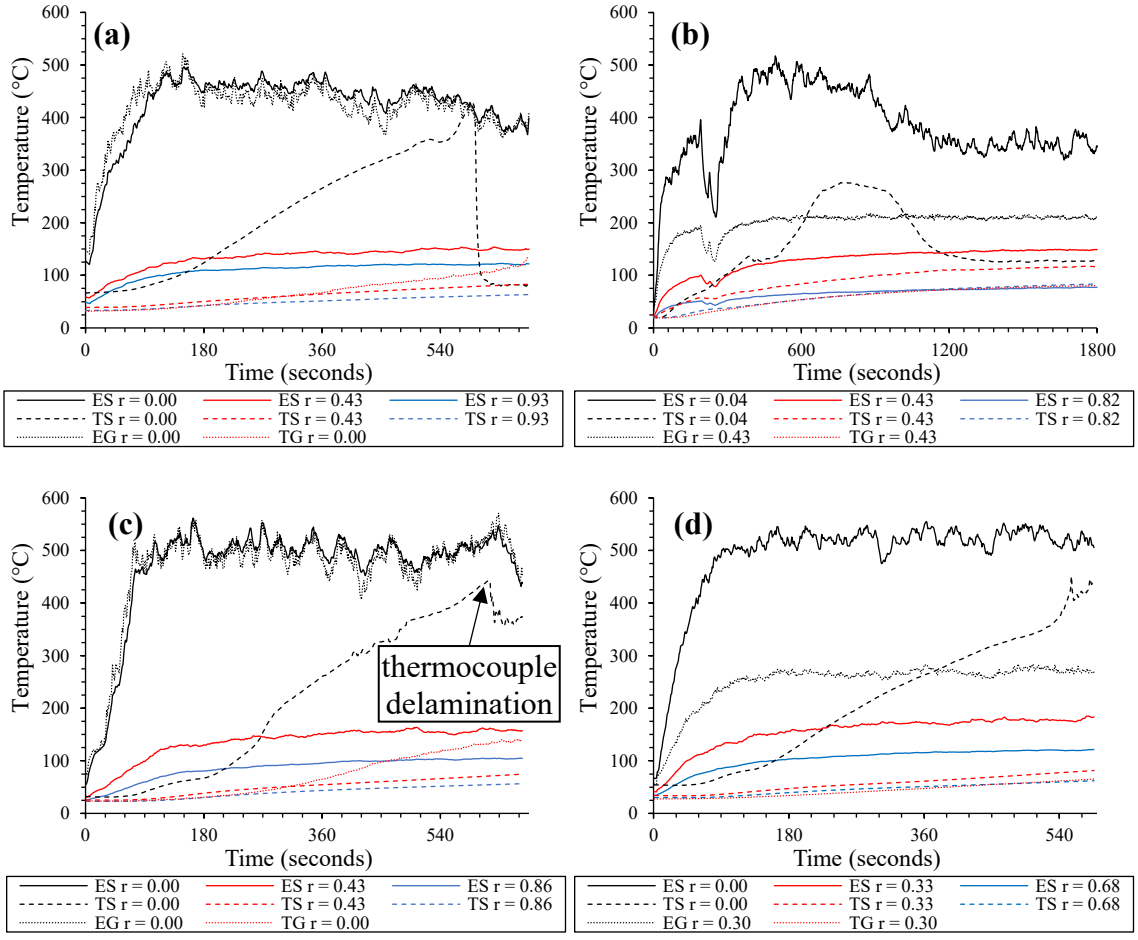

Figure 17 Temperatures observed during testing: (a) Test 1; (b) Test 2; (c) Test 3 with sample of unexposed side surface thermocouple delamination; and (d) Test 4.

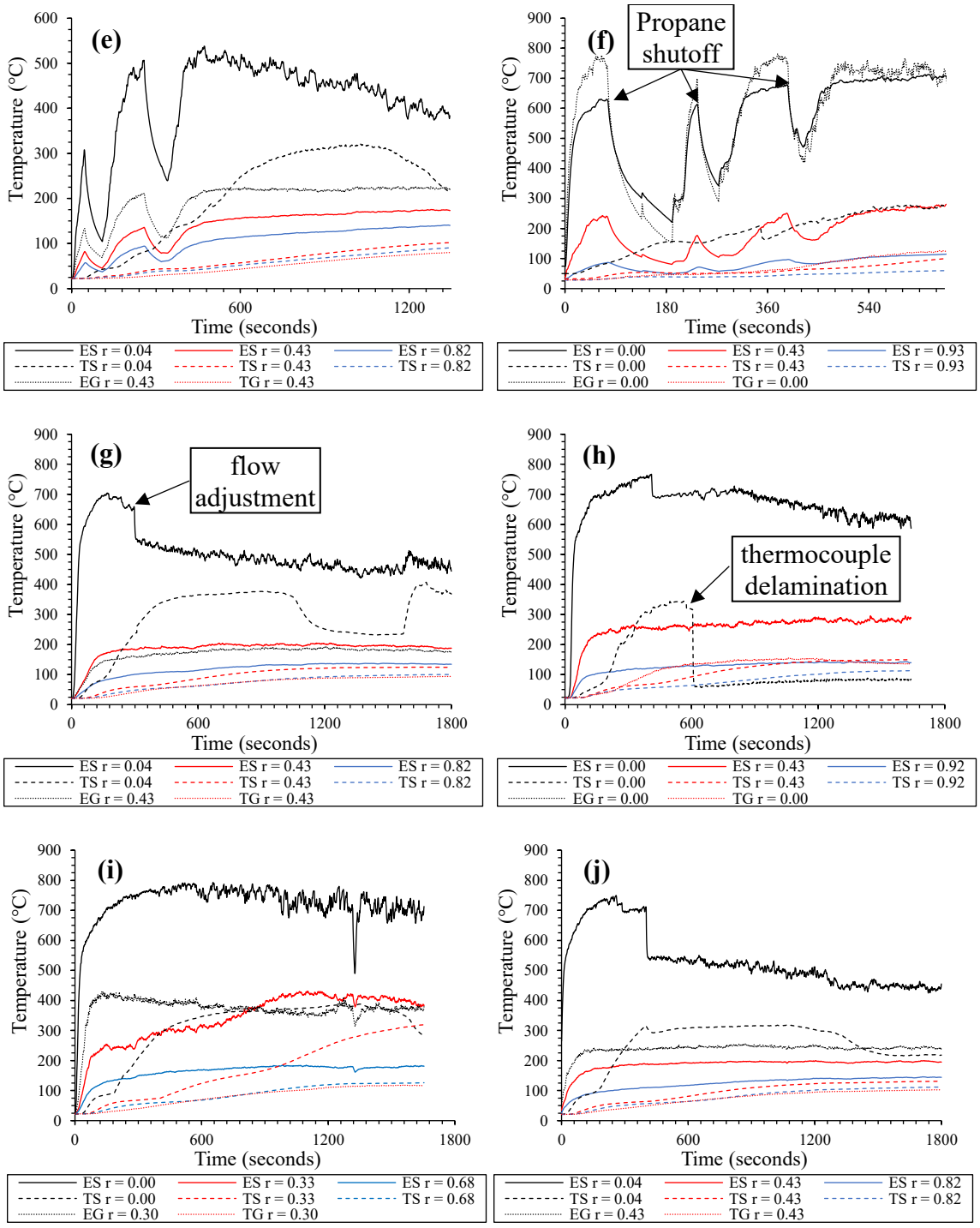

Figure 18 Temperatures observed during testing: (e) Test 5; (f) Test 6 with sample of propane auto shut-off; (g) Test 7 with sample of flow adjustment; (h) Test 8 with sample of unexposed side surface thermocouple delamination; (i) Test 9; and (j) Test 10.

Several issues occurred during the tests and have been identified in Figure 17 and Figure 18. One issue observed was that automatic shut-off of the propane tank occurred due to the internal flow limiting device (a common safety feature in such tanks) activating. Further to this, the maximum flow from the tank slowed during testing due to cooling of the tank regulator resulting in a slightly lowered heat release rate at the end of the test when compared to the start (in the worst instance, the flow reduced to 9.53 SLPM after a 30 minute period). Delamination of the unexposed-side surface thermocouples was also observed above the burner location; however, this was corrected in most tests through the use of foil-tape to help bond the thermocouple throughout the test. Finally, a common issue was a need to readjust the flow rate of propane after the first few minutes of testing. To address these issues, it is recommended that future research in this area employ the use of multiple propane tanks manifolded together (to limit the flow from each individual tank and provide a more constant heat release rate) and to explore other options for measuring surface temperatures on the unexposed side of the NCTS.

Higher temperatures were observed during the tests in which a 250 mm height between the burner and the above tiles was used. Another trend is that during both the 250 mm and 500 mm tests higher temperatures were observed for the tests in which the burner was located on the centre of a tile (RR or RC), or conversely, the tests in which the burner was located closer to the walls of the apparatus. This trend indicates that the proximity of the burner to the walls of the apparatus has an impact on the observed ceiling temperatures during tests. This behaviour was expected but not specifically explored in this work.

7.1.2 Time to Failure

As previously noted, failure of the ceiling tile systems was defined as the point where flame breakthrough into the cavity above was observed during the testing. Once failure had occurred during the test, flaming through the tile was not consistent in all cases; with flames typically flickering up through cracks in the tile periodically. Sample images for Test 3 and Test 6 before and after flame breakthrough are provided in Figure 19.

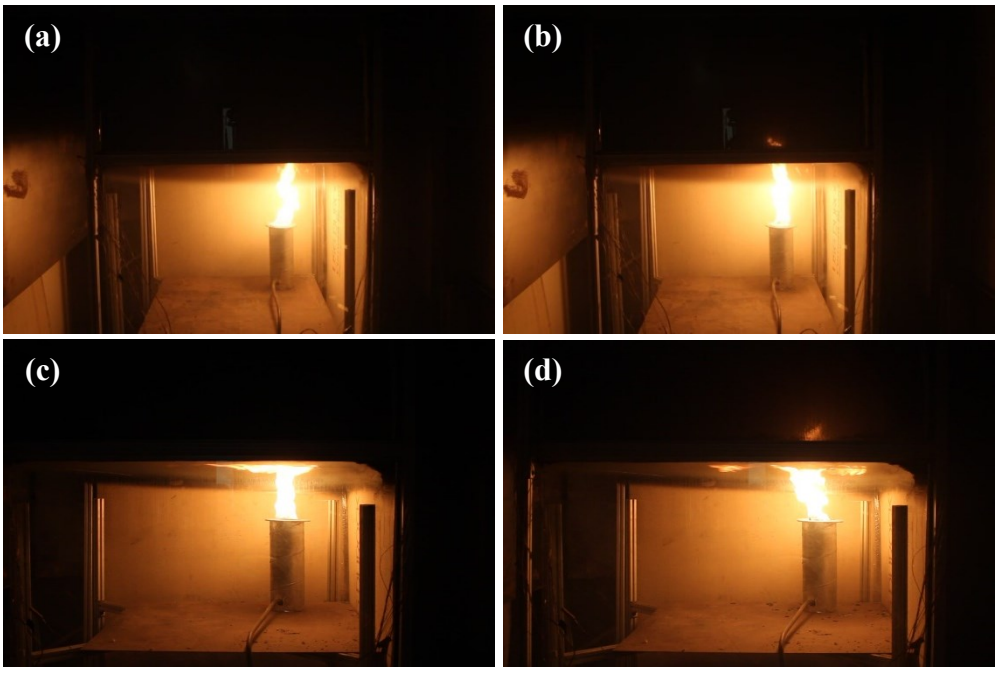

Figure 19 Examples of flame breakthrough, taken from (a) Test 3 prior to failure; (b) Test 3 after failure; (c) Test 6 prior to failure; and (d) Test 6 after failure.

Across the series of tests, failure was only observed to occur during Tests 1, 3, 4, and 6, all of which included the burner being located beneath the centre of a tile. It is noted, however, that failure was not observed in every test where the burner was located beneath the centre of a tile, as failure did not occur during Tests 8 and 9. The failure results and times to failure are provided in Table 3.

Table 3 Failure results for each test and the average times to failure (where observed).

Test #	Failure (Yes/No)	Time to Failure (seconds)
1	Yes	675
2	No	–
3	Yes	665
4	Yes	586
5	No	–
6	Yes	829
7	No	–
8	No	–
9	No	–
10	No	–

The first trend that emerges is that failure of the NCTS only occurred in instances where the burner was located directly below the centre of a tile, and that failure was not observed when the burner was located beneath the intersection of the framing members. As discussed in Section 7.1.3, failure of the NCTS appeared to occur due to the ceiling tile losing its structural integrity, and the framing members appeared to provide a level of support that prevented failure from occurring. Based on this it appears that failure of the NCTS is dependent on the location of the heat source and that failure will be more likely to occur when the heat source is located directly below the centre of a tile.

Across all tests where failure occurred, a minimum time to failure of 586 seconds was observed. The average time to failure for the NCTS across all tests was 689 seconds, with a standard deviation of 102 seconds. Based on these results it appears that the expected time to failure for a NCTS is between 477 and 901 seconds (calculated using a Student-t distribution at a confidence of 95%). Looking at the tests individually, it is noted that the

time to failure where a 500 mm height was used (Tests 1, 2, and 4) are closer in value and significantly shorter than the time to failure using a 250 mm height (Test 6). This appears to indicate that there may be a relation between the height of the NCTS above the burner.

To test for a relationship between time to failure and height of the NCTS above the burner it is noted that looking specifically at the tests using a 500 mm height yields an average time to failure of 642 seconds with an expected time to failure for a NCTS being between 467 and 817 seconds (calculated using a Student-t distribution at a confidence of 95%). The time to failure using a 250 mm height (829 seconds) falls just outside of this expected time to failure when using a 500 mm height. Further to this while the lower-end of this confidence interval remains relatively constant (477 seconds compared to 467 seconds), it is noted that the upper end of this confidence interval changes significantly (901 seconds compared to 817 seconds). Based on these results there appears to be a strong possibility of a relationship between time to failure and height of the NCTS above the burner. However, due to the limited number of tests and issues with Test #6 as previously noted in Section 7.1.1, this relationship cannot be precisely quantified and is an area that should be explored in further research. It is noted that in all cases, failure of the NCTS is not expected to occur within the first 467 seconds of testing.

With respect to the time to failure based on the burner location, it is noted that Test 3 and 4, which both used a 2-tile arrangement, were observed to have the lowest times to failure of all tests where failure was observed. Based on the above discussion regarding the support provided by the framing members as discussed in section 7.1.3, this result is expected as the 2-tile arrangement has the least amount of support provided by these members. Furthermore, as discussed in section 7.1.1, Test 1, 3, and 4, which had a burner located at

either the RR or RC location, had higher observed exposure temperatures than those with the burner located at the C location which may also have attributed to failure only being observed during these tests.

7.1.3 Endpoint Condition of Tiles

In addition to time to failure, an important factor to determine is the mode of failure of the NCTS (where observed) and the condition of the individual tiles at the end testing where failure was not observed. As previously noted, failure of the NCTS was only observed to occur during Tests 1, 3, 4, and 6. Sample images of the condition of the tiles from these tests are provided in Figure 20.

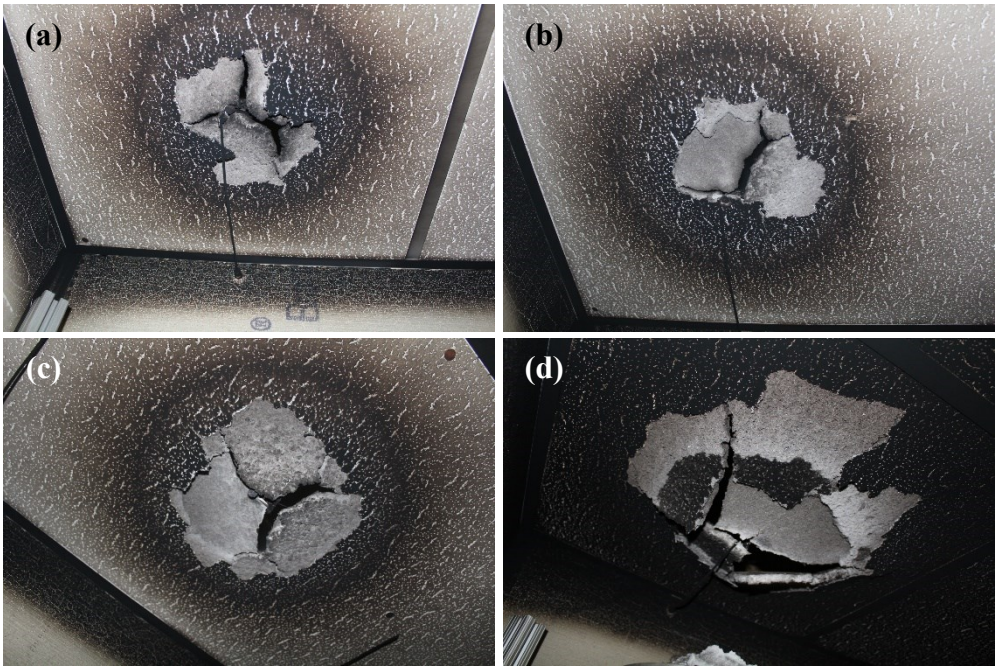

Figure 20 Endpoint condition of NCTS where failure was observed during testing: (a) Test 1; (b) Test 3; (c) Test 4; and (d) Test 6.

Looking at the images in Figure 20, it is apparent that failure of the NCTS occurred due to cracking of the tile above the burner location, with delamination of the exterior surface of

the tile, charring, and soot accumulation also being observed on the fire exposed side. Furthermore, sagging of the NCTS in the cracked areas of the tile was observed and is shown in Figure 21.

Significant sagging was not observed where failure of the NCTS did not occur. Sample images of the endpoint condition of the tiles from these tests are provided in Figure 22.

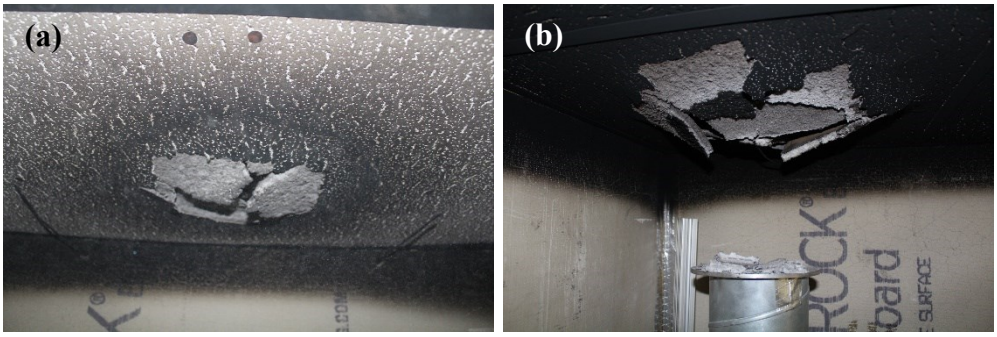

Figure 21 Side view of NCTS where failure was observed demonstrating sagging of the ceiling tile material for (a) Test 4; and (b) Test 6.

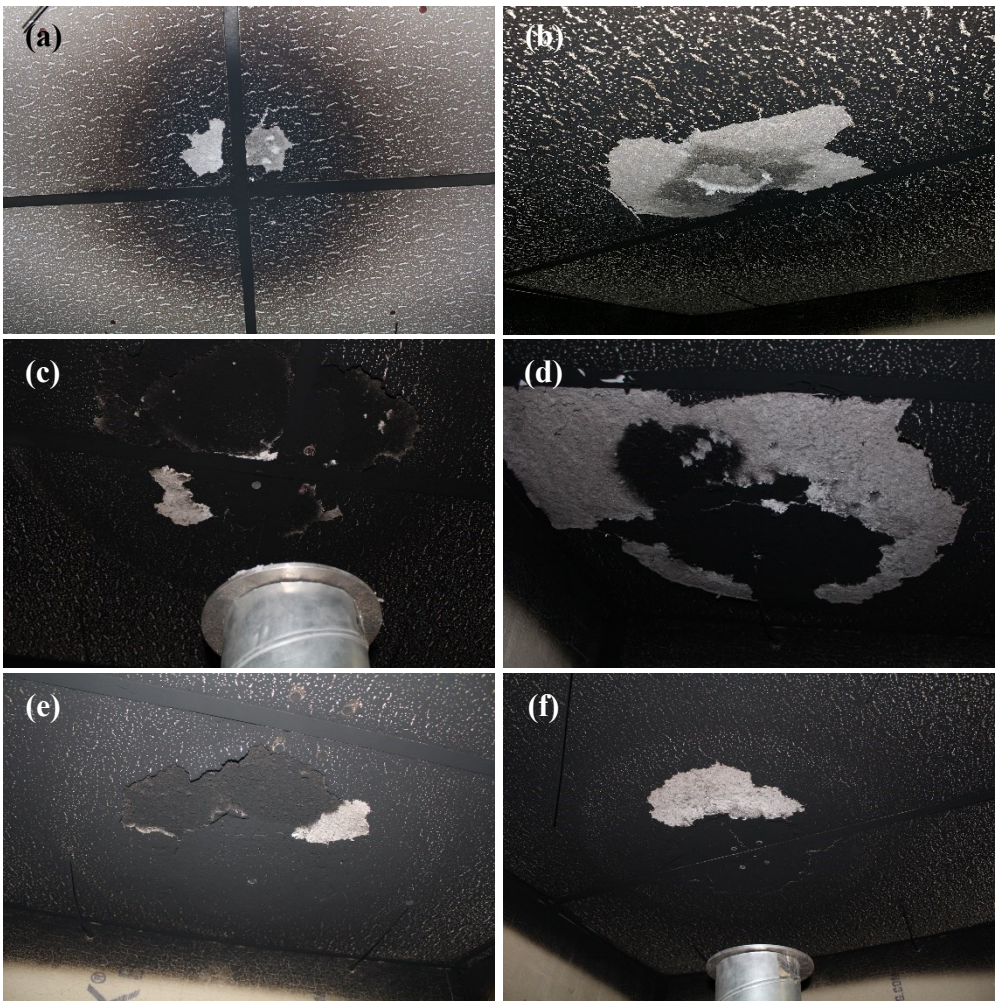

Figure 22 Endpoint condition of ceiling tiles where failure was not observed during testing: (a) Test 2; (b) Test 5; (c) Test 7; (d) Test 8; (e) Test 9; and (f) Test 10

As can be seen from the images of each test, by the end of each test the NCTS had all experienced an accumulation of soot, charring, and delamination of the exterior surface on the fire-exposed side of the tiles. More significant charring and delamination was observed the closer the heat source was to the underside of the tile. Further to this, in each case a clearly defined circular area above the burner was observed to experience heavier charring when compared to the remainder of the NCTS. While the size of this area appears to be larger where a smaller height above the burner was used, this area is not as clearly pronounced due the increased level of soot accumulation and charring.

With respect to the condition of the tile material at the end of each test, the area directly above the burner was found to be very fragile/delicate. This area of the tile, approximately the same size as the heavily charred circle, had an almost dust-like consistency and could be easily removed with a pen or finger as shown in Figure 23.

Figure 23 Endpoint condition of the NCTS from Test 2, with the delicate areas of the tile removed using minimal force by a pen.

It is apparent that the tiles themselves degrade and lose their material strength as the tests progress and that the framing elements provide support for the tile material itself. This result is expected as degradation of the tile, volatilization of the material components, and moisture loss would be expected at the temperatures observed on both the exposed and unexposed sides of the tiles. Furthermore, it is understood that onset of the degradation of glass fibres has been observed to occur in testing around 250 °C, as discussed by Thomason et al [27]. Based on these results and associated discussion, it appears that failure of the NCTS occurs due to the tile losing its structural integrity and degrading to the point where it can no longer support its own weight. Where the burner was located in the centre of the apparatus, the framing members appeared to provide a level of support and prevent failure of the NCTS from occurring.

7.2 THERMAL RESISTANCE PROVIDED PRIOR TO FAILURE

This section explores the thermal resistance provided by the NCTS and the rate of heat transfer through the tiles prior to failure. As part of this analysis, the following sections present observed surface temperature distributions, average gas temperatures above and below the NCTS, and calculated rates of heat transfer through the NCTS. To provide a consistent reference for comparing the performance characteristics of the tiles prior to failure across all tests, and in keeping with the expected time to failure for a NCTS discussed in Section 7.1.2, the results for each test presented in the following sections have been compared at a time of 477 seconds. The presented values were averaged over the prior 30 seconds of testing. This is representative of a time in advance of when failure was observed during testing but at the beginning of the confidence interval for the expected time to failure across all tests.

7.2.1 Surface Temperature Distributions

Surface temperature distributions are an important characteristic to quantify as part of evaluating the thermal resistance provided by a NCTS prior to failure. Knowing the surface temperature distributions on the exposed side and top side of the NCTS can provide insight into heat transfer as a function of radius and allows for comparison of the exposed side temperature against existing models (such as the Alpert model [25]). Furthermore, knowing the temperature difference across the tile as a function of radius can be used to estimate the instantaneous rate of heat transfer through the tile at a given point. Figure 24 and Figure 25 present the temperature distributions on the exposed and top side of the tiles during each test averaged from 447–477 seconds as a function of radius. For comparison purposes, the

corresponding calculated exposed side surface temperatures have also been included using the Alpert model as presented by Drysdale using Equations 3 and 4 with a heat release rate of 13.5 kW.

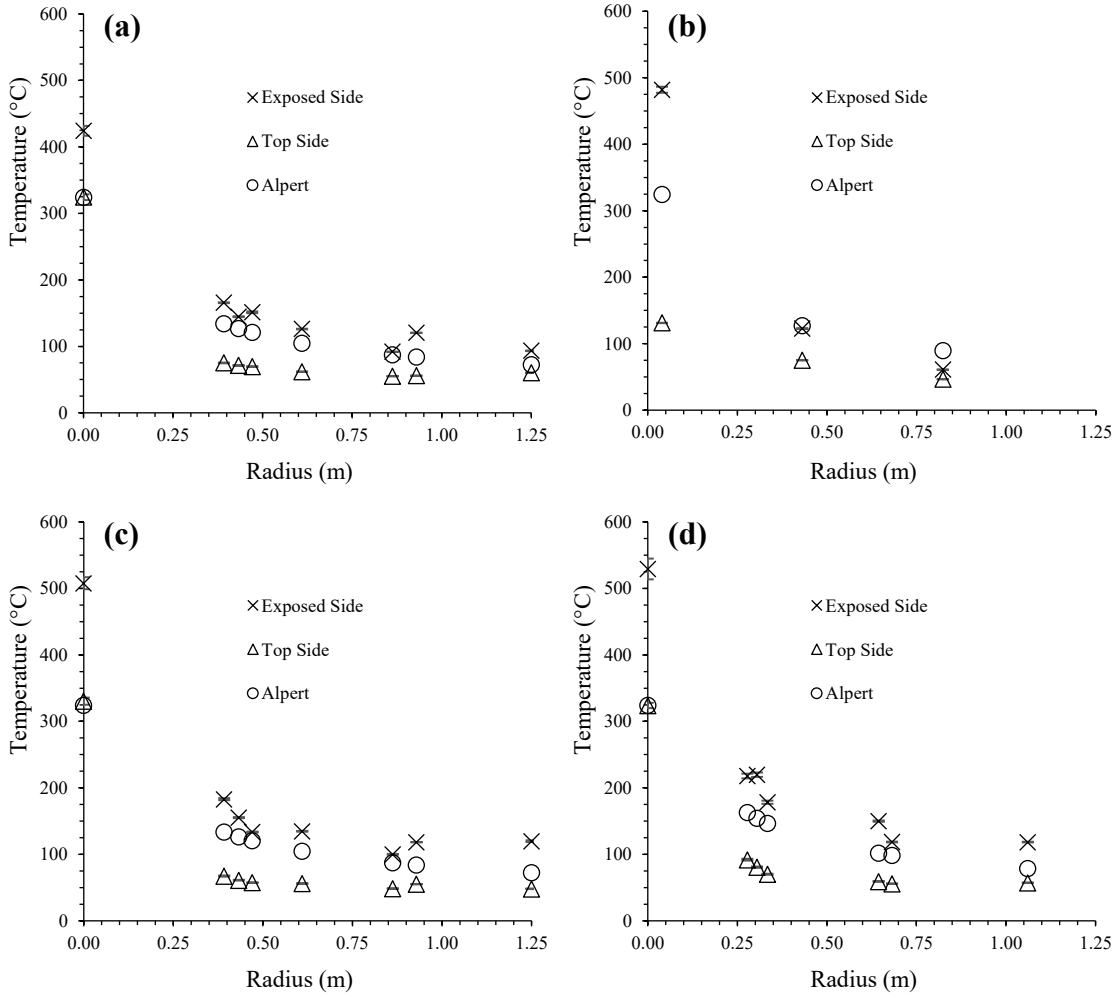

Figure 24 Surface temperatures observed prior to failure averaged from 447–477 seconds (with error bars representing one standard deviation) for (a) Test 1; (b) Test 2; (c) Test 3; and (d) Test 4.

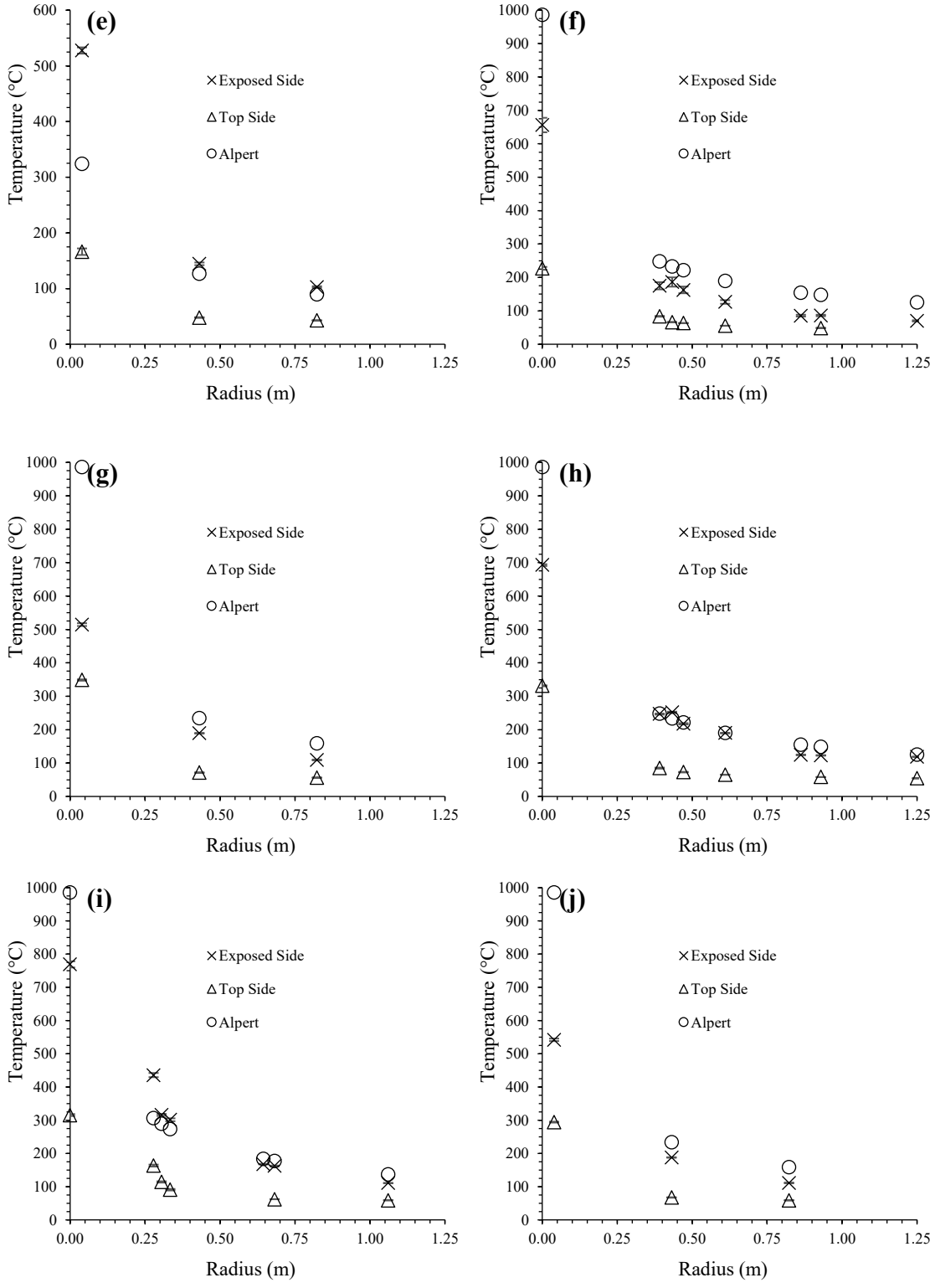

Figure 25 Surface temperatures observed prior to failure averaged from 447–477 seconds (with error bars representing one standard deviation) for (e) Test 5; (f) Test 6; (g) Test 7; (h) Test 8; (i) Test 9; and (j) Test 10.

As can be seen in Figure 24 and Figure 25, the temperature distributions appeared to be relatively constant on the exposed side for tests taken at the 500 mm height. However, for the tests taken at the 250 mm height, the location of the burner appears to have a larger impact on the exposure temperatures, specifically those directly above the burner.

With respect to the comparison of these results against the Alpert model, is noted that exposure temperatures appear to be under-predicted for the tests having a height between the burner and tiles of 500 mm, and that exposure temperatures are significantly over-predicted for the tests at a height of 250 mm. To compare the observed temperature profiles against those expected using the Alpert model, which as shown in Equation 3 are expected to be proportional to $r^{-2/3}$, the observed temperature increases above ambient have been plotted against the radial distance from the centreline of the burner on a log-log plot in Figure 26.

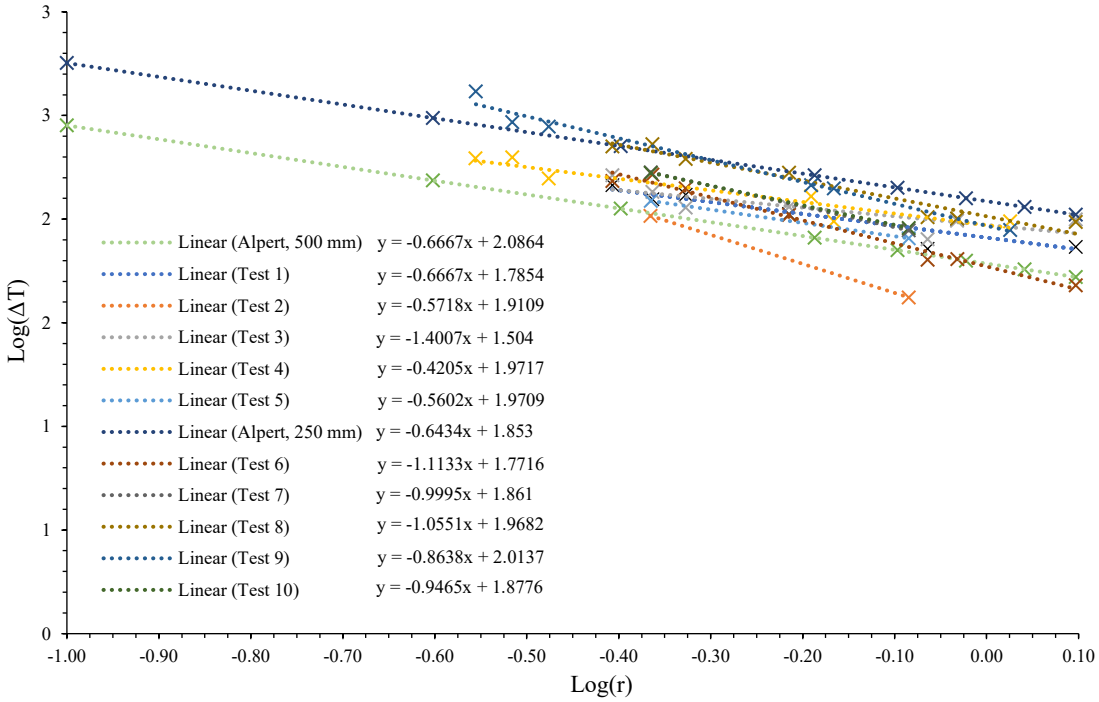

Figure 26 Log-Log plot of the observed temperature increase above ambient for all tests averaged from 447–477 seconds against radial distance from the centreline of the burner.

From the trendlines shown in Figure 26, it can be seen that for the 500 mm tests (except for Test 2) the slopes of the trendlines are between -0.42 to -0.64 showing that these tests tend to generally follow the Alpert profile which has a slope of -0.67 (as expected for the expression in Equation 3). For tests 6 to 10, the slopes of the trendline are between -0.86 to -1.11, showing that the temperature profiles in these tests significantly deviate from those expected by the Alpert model. Overall, these results when compared against the Drysdale model can be expected as, for the 500 mm height tests ($l/H = 1.1$), there was minimal impingement and the heat release rate used for the model has not been adjusted to account for the proximity of walls to the fire and associated effect on the entrainment of air into the fire plume. Regarding the 250 mm height tests ($l/H = 2.2$), the significant over-prediction of the exposure temperatures and deviation from the expected temperature

profile can be expected because, when significant flame impingement is observed, i.e., ($l/H > 2$), Alpert's model begins to break down.

To describe the thermal resistance provided by the tiles prior to failure, temperature differences between the exposed and unexposed sides of the tiles averaged from 447–477 seconds for each test are provided in Figure 27 as a function of radius. Discussion regarding the rate of heat transfer through the tiles is provided in Section 7.2.3.

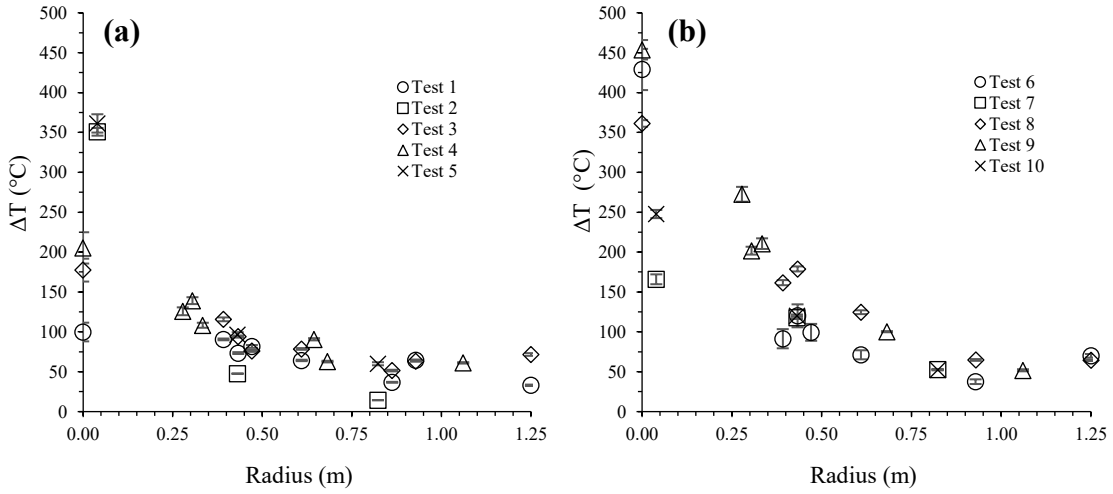

Figure 27 Temperature differences between the exposed and unexposed sides of the tiles averaged from 447–477 seconds (with error bars representing one standard deviation) for (a) tests at a height of 500 mm and (b) tests at a height of 250 mm.

In general, it is noted that the temperature difference through the tiles within a radius of 500 mm of the burner tended to be between 100 °C to 450 °C. Outside a radius of 500 mm from the burner, observed temperature differences appears to converge and level out around 50 °C to 125 °C. Observed temperatures directly above the burner and the impact of the burner location is discussed further in Section 7.3. Averaged across all tests, an average surface temperature difference over the entire area of the tiles of 134 °C was

observed between the exposed and unexposed sides. To observe the effect of individual parameters, the average temperature differences for each burner location and height have been compared in Figure 28.

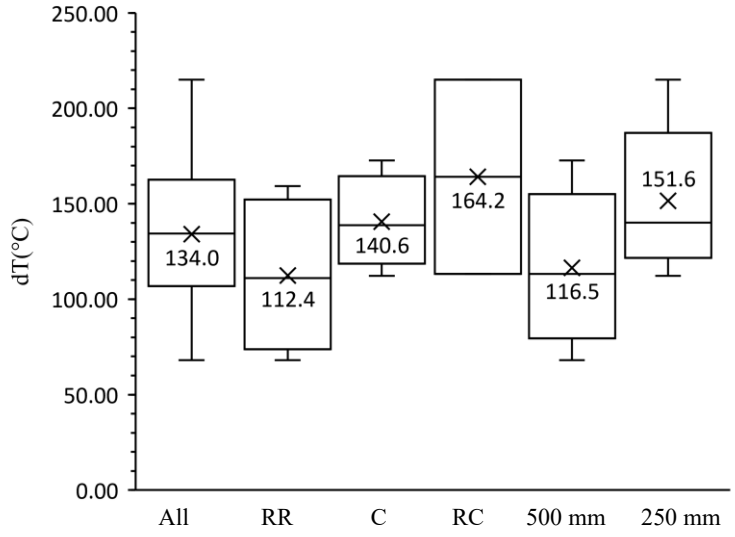

Figure 28 Average temperature differences over the entire tile area between the exposed and unexposed sides of the tiles averaged from 447–477 seconds compared for each burner height and location. Mean values are represented by an "×", outlying data points are noted by the outer bounds, and the box represents the first through third quartile of data points.

There appears to be a relationship between the average temperature difference across the tiles and both the height and location; however, this relationship is difficult to quantify due to the limited number of tests and the close range of observed values. While not specifically covered as part of this research, this is an area that could be explored in further research.

7.2.2 Average Gas Temperatures

To provide further analysis of the thermal resistance provided by the tiles prior to failure, the average gas temperatures on the exposed and unexposed sides of the tiles averaged from 447–477 seconds for each test have been compared and are presented in Figure 29.

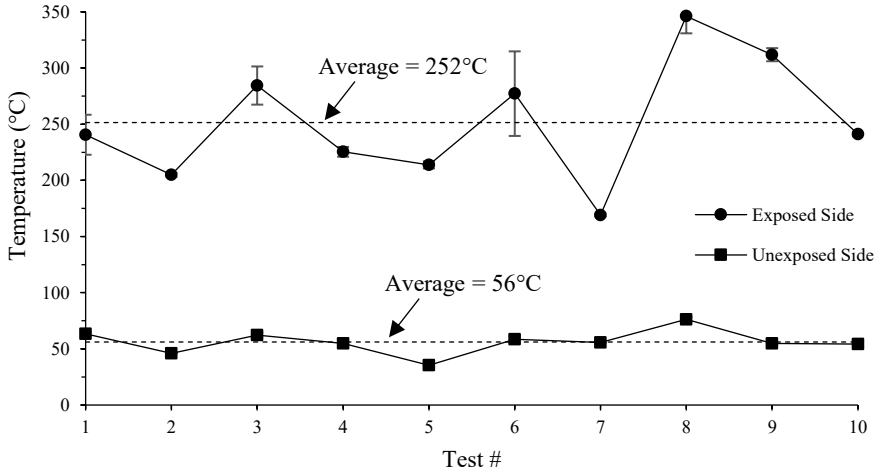

Figure 29 Average gas temperatures on the exposed and unexposed sides of the tiles averaged from 447–477 seconds (with error bars representing one standard deviation) for each test.

When averaged across all tests, the average gas temperature on the exposed side of the tiles was found to be approximately 252°C (standard deviation of 53°C, n = 10). It is noted, however, that there is significant variability, with individual values ranging between 169°C and 346°C. Unlike the exposed side, average gas temperatures on the unexposed side were relatively constant, having an average of 56°C (standard deviation of 11°C, n = 10) and individual values ranging from 35°C to 76°C. On average, the gas temperatures on the exposed sides of the tiles were found to be 195°C higher than the gas temperature on the unexposed side. To observe the effect of individual parameters, the average temperature differences for each burner location and height have been compared in Figure 30.

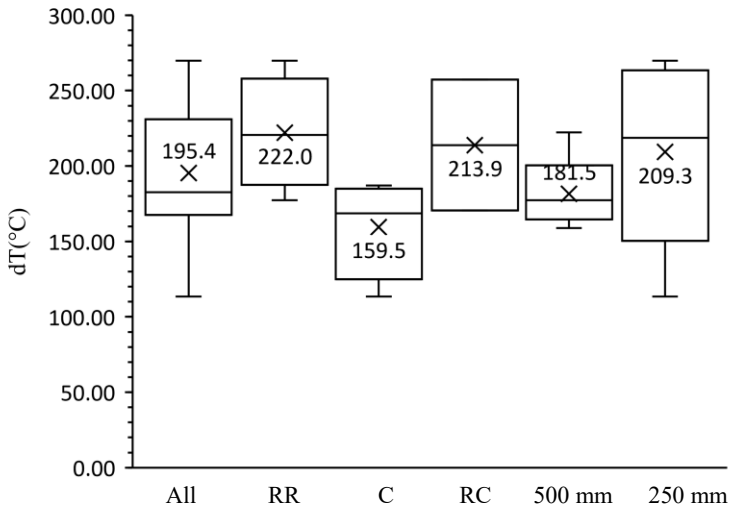

Figure 30 Average gas temperature differences over the entire tile area between the exposed and unexposed sides of the tiles averaged from 447–477 seconds compared for each burner height and location. Mean values are represented by an "×", outlying data points are noted by the outer bounds, and the box represents the first through third quartile of data points.

Comparing these values against the average surface temperature discussed in Section 7.2.1, it is first noted that the average gas temperature difference across all tests was higher than the observed average surface temperatures, 194°C and 134°C respectively. This would be expected, as heat is transferred via conduction through the tiles and then through convection to the cavity on the unexposed side. With respect to the impact of individual parameters, comparing the results presented in Figure 28 and Figure 30 two trends appear: tests with a burner located at the centre of the apparatus had a smaller temperature difference across the tiles compared to tests with a burner located at the right centre of the apparatus; and similarly, tests with a burner located at a 500 mm height had a smaller temperature difference across the tiles compared to tests with a burner located at a 250 mm height.

The impact of the burner location could be expected as having the burner at the right centre of the apparatus would allow the heated plume to travel further along the ceiling tile before exiting the apparatus. Furthermore, the burner being closer to the wall of the apparatus would increase gas and surface temperatures on the exposed side which both then drive a higher temperature difference. Regarding the burner height, this would also be expected as exposure temperatures were higher for the tests with a burner height of 250 mm.

7.2.3 Heat Transfer Through Tiles

One aspect explored as part of this research is the rate of heat transfer, $\dot{Q}$ (kW), through the NCTS (in this case specifically between a time of 447–477 seconds). Due to the nature of the experiments and equipment used this can be difficult to determine, but it is possible to approximate this value. Using the observed temperature differences across the NCTS and the known tile properties (as presented in Table 1), the heat flux, $\dot{q}''$ (kW m^{-2}), at a given point through the tile can be estimated using Equation 5. Following this approach, heat flux through the tiles averaged from a time of 447–477 seconds was calculated for each test and are provided in Figure 31 as a function of radius.

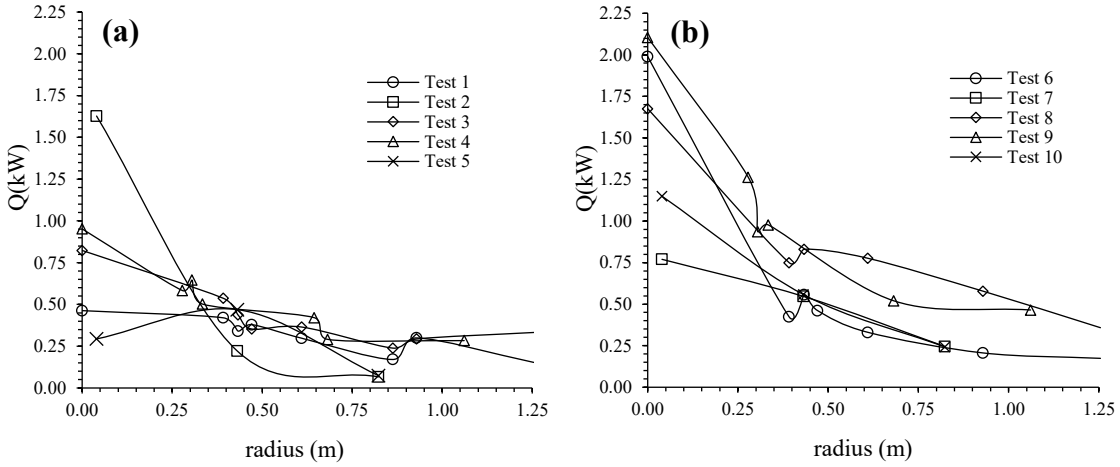

Figure 31 Calculated heat flux, $\dot{q}''$ (kW m^{-2}), through the tiles as a function of radius at a time of 477 seconds for (a) tests at a height of 500 mm and (b) tests at a height of 250 mm.

With the calculated values for heat flux and the area (m^2) of the tiles known, the rate of heat transfer through the tile could be estimated/averaged across the entire tile. It is noted, however, that applying such an approach is not as straightforward as it may seem and presents issues as the calculated heat flux varies as a function of radius and the spacing of the radii where points are known (i.e., the location of each thermocouple with respect to the burner) varies. To address this, the heat transfer through the tiles has been approximated using an integration-by-parts; wherein the total area of the tile was broken into discretized areas bounded by the halfway point between each of the radii used for each burner location. A visual representation of these discretized areas is provided in Figure 32.

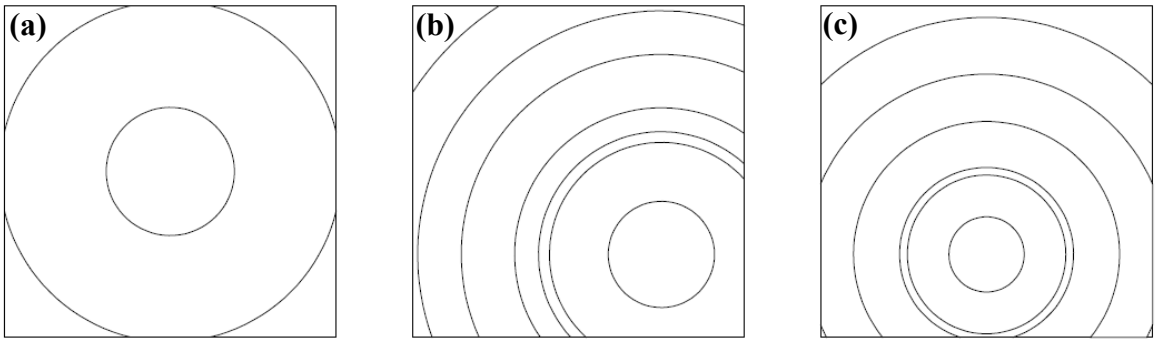

Figure 32 Representation of discretized areas used as part of an integration-by-parts to calculate heat transfer through the NCTS for burner locations (a) at the centre; (b) right rear; and (c) right centre of the apparatus.

The total rate of heat transfer through a NCTS averaged from 447–477 seconds was then calculated by taking the sum of each discretized area multiplied by its respective heat flux for each test. The total calculated heat transfer rates for each test are provided in Table 4.

Table 4 Calculated heat release rate, $\dot{Q}$ (kW), through the NCTS averaged from 447–477 seconds for each test, compared against the burner heat release rate.

Test #	Heat Transfer Rate $\dot{Q}$ (kW)	% of Burner HRR
1	0.471	3.49%
2	0.534	3.95%
3	0.604	4.48%
4	0.672	4.98%
5	0.836	6.20%
6	0.685	5.07%
7	0.773	5.72%
8	0.958	7.09%
9	1.141	8.45%
10	0.850	6.30%

The average rate of heat transfer through the NCTS across all tests averaged from 447–477 seconds was found to be 0.752 kW (standard deviation of 0.203, n = 10), equivalent to approximately 5.57% (standard deviation of 1.50%, n= 10) of the total heat release rate of the burner during the tests (13.5 kW). To compare the effect of individual parameters, the average heat transfer rate through the NCTS for each burner location and height are provided in Figure 33.

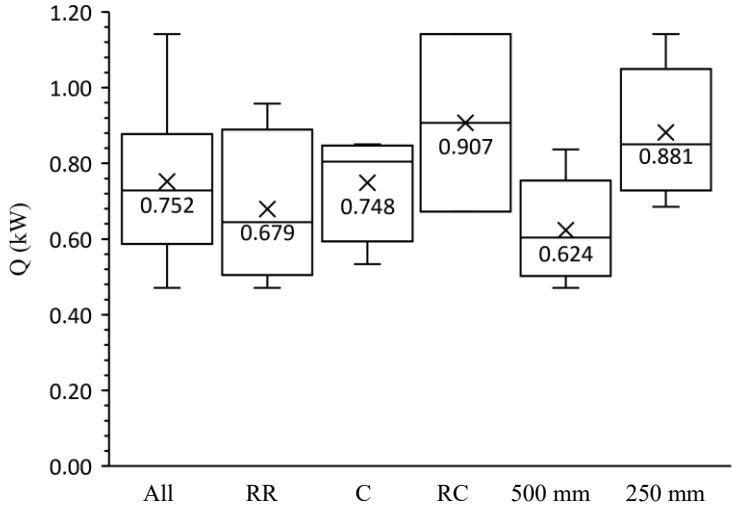

Figure 33 Average calculated rates of heat transfer through the NCST averaged from 447–477 seconds compared for each burner height and location. Mean values are represented by an "×", outlying data points are noted by the outer bounds, and the box represents the first through third quartile of data points.

There appears to be a relationship between the calculated heat transfer rate through the tile and both the burner location and height. While this relationship appears to be more significant for the different burner heights, this relationship is difficult to quantify due to the limited number of tests and range of data points. While not specifically covered as part of this research, these relationships should be explored in further research.

7.3 Observed Temperatures at Burner Location

As part of determining failure criteria, an important aspect to explore is the observed surface temperatures on the fire-exposed side and the unexposed sides of the NCTS directly above the burner. This section discusses observed surface temperatures directly above the burner at the time of failure or, where failure was not observed, at the average expected time to failure (689 s as discussed in Section 7.1.2) and at the end of the testing period. The values presented have been averaged over the prior 30 seconds of testing to provide a more accurate representation of the actual observed temperatures. Due to the location of the gas-phase thermocouples during testing it is noted that only Tests 1, 3, 6, and 8 had these devices located directly above the burner and as such (due to the limited number of data points to compare), have not been explored in this section. It is recommended that future research consider the use of gas-phase thermocouples located directly above the burner location for each testing scenario.

Observed surface temperatures directly above the burner for the conditions described above are presented in Figure 34 and Figure 35, with outlying data points (caused by delamination of the unexposed-side surface thermocouple, as discussed in Section 7.1.1) identified with a hollow data marker.

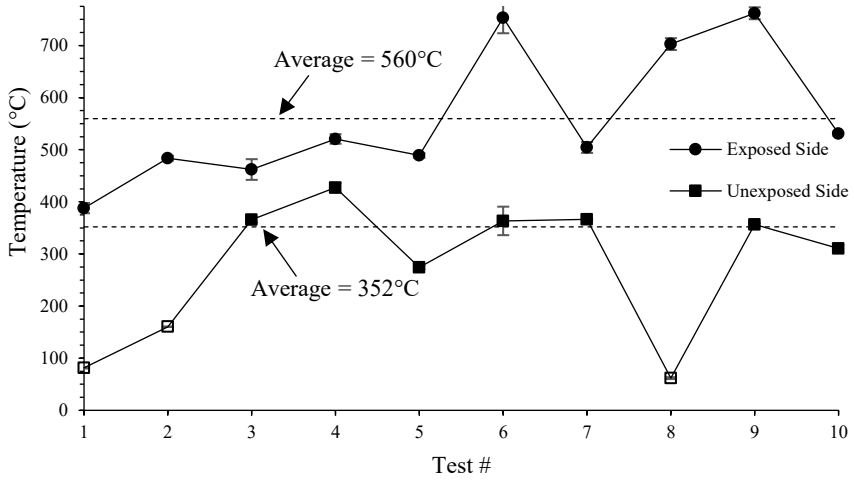

Figure 34 Observed surface temperatures at $r = 0.0$ m at failure or, where failure was not observed, a time of 689 s (with error bars representing one standard deviation). Outlying data points are identified with a hollow marker.

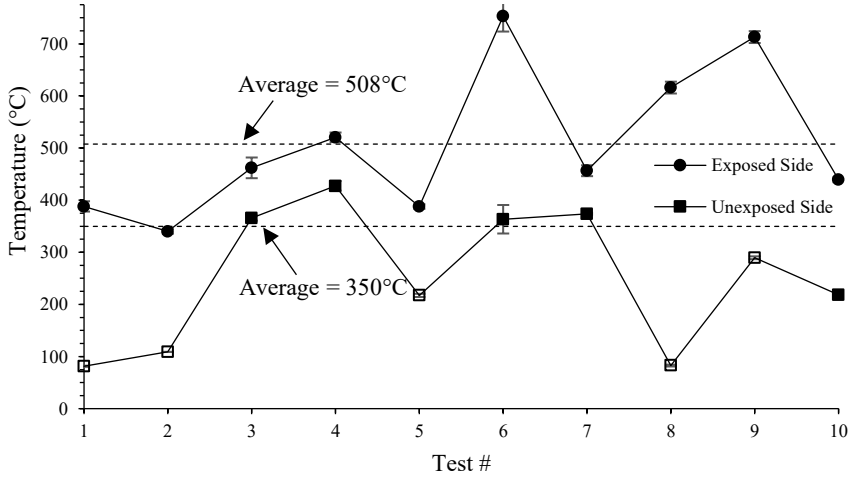

Figure 35 Observed surface temperatures at $r = 0.0$ m at failure or, where failure was not observed, at the end of the testing period (with error bars representing one standard deviation). Outlying data points are identified with a hollow marker.

Averaged across all tests at the time of failure, surface temperatures on the fire-exposed side of the NCTS were observed to be 560°C (standard deviation of 131°C, n=10), surface temperatures on the unexposed side (not including outlying data points as discussed above) were observed to be 352°C (standard deviation of 48°C, n=7), and the average observed

temperature difference was 223°C (standard deviation of 130°C, n=7). Surface temperatures on the unexposed sides (with outliers removed) were noted to remain relatively constant across all tests when compared to the surface temperatures on the exposed side, as shown by the large difference in the standard deviation of the average values (48°C compared to 131°C). With respect to the surface temperature differences between the exposed and unexposed sides, a larger temperature difference was observed for the 250 mm tests; however, as the unexposed side surface temperatures remained relatively constant, this increased temperature difference for the 250 mm test is primarily attributed to the higher observed exposure temperatures.

Regarding the results at the end of the testing sequence, it is noted that the average surface temperatures on the exposed and unexposed sides were observed to be lower than at the time of failure. This would be expected because, as noted in Section 7.1.1, temperatures throughout each test tended to decrease near the end of testing due to a reduction in the flow rate of propane caused by cooling of the tank valve. Overall, a large decrease in the exposure temperatures on the unexposed side (560°C at the time of failure, 508°C at the end of testing) was observed, but surface temperatures on the unexposed side remained relatively constant (352°C at the time of failure and 350°C at the end of testing). This appears to indicate that the heat transfer rate and thermal resistance through the tile had achieved a relatively steady state. With respect to future testing, as previously noted in Section 7.1.1, consideration should be given to the means used to attach the unexposed-side surface thermocouples as there were a significant number of outlying data points on the unexposed sides of the tiles.

CHAPTER 8 NUMERICAL STUDY

The primary application of this research is to provide quantitative data to assist in the inclusion of NCTSs within fire models, such as FDS models. As such, there is added benefit in knowing the extent to which a numerical model is capable of predicting the expected results of a given fire scenario. To provide a comparison between observed and predicted results, a model representing the conditions of Test 3 has been created using Pyrosim [34], a FDS visualizer and modelling software. The following sections describe the FDS model, the sensitivity analysis completed, and provide a comparison between the experimental and numerical results.

8.1 DESCRIPTION OF MODEL

For the purpose of comparing the experimental test results against a numerical model, Test 3 was selected as failure was observed during this test near the average time to failure, minimal issues were observed with respect to devices (i.e., the propane did not shut-off during the beginning of testing and delamination of a surface thermocouple only occurred near the end of the testing period), and relatively constant temperatures were observed throughout the test. As previously noted, the numerical model representing Test 3 was created using Pyrosim. Figure 36 provides a sample image of the Pyrosim model and interface.

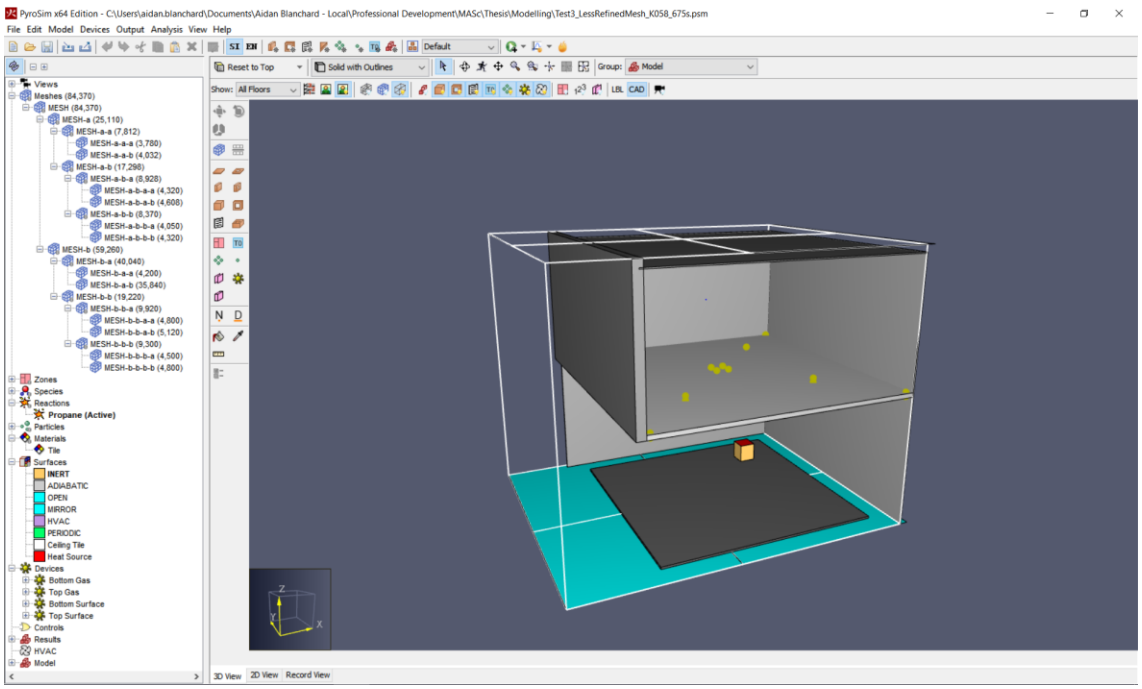

Figure 36 Sample image of Pyrosim model of Test 3 and Pyrosim user interface. A red surface represents the heat source with individual devices represented by yellow spheres.

To create the model, the Z_{min} and Z_{max} boundaries were assigned as open vents to allow the free passage of air and combustion products in/out of the model, which is representative of the apparatus being open to the room at the bottom and combustion products being vented through the extraction hood. The cement board and steel plate portions of the test apparatus were represented using adiabatic surfaces because heat transfer through these materials is expected to have a negligible effect on the heat transfer through the ceiling tiles, and the ceiling tiles were represented using the material properties discussed in Section 4.5. For the purpose of this model, the steel plate was located within the domain such that its impact on airflow and entrainment into the apparatus could be represented, with a single grid space (40 mm) provided between the top of the apparatus and Z_{max} boundary. In determining the heat transfer rate through the ceiling tiles, a one-dimensional model was used for heat

transfer through solids. A surface boundary must be specified for any materials involved in such calculations. For the purpose of this model the top and bottom surfaces of the ceiling tile have been considered to be exposed to the surrounding gas-phase environment and the unexposed edges of the tiles have been represented as adiabatic surfaces.

A total of 12 individual meshes were used within the model (as discussed further in Section 8.2), with the mesh directly around the burner and those within 40 mm (above and below) of the bottom of the NCTS having a grid size of 20 mm (five total). The remaining meshes within the model were assigned a grid size of 40 mm (seven total). This approach was chosen to provide a greater resolution in the areas directly surrounding the fire plume and where there is interaction between the gas- and solid-phase heat transfer surrounding the NCTS. The location of meshes with respect to their assigned grid size is shown in Figure 37.

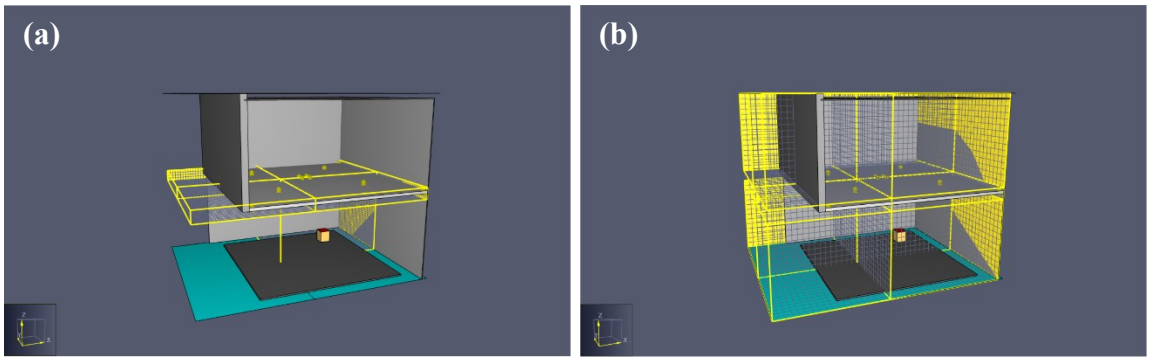

Figure 37 Location of meshes having a grid size of (a) 20 mm and (b) 40 mm.

For the model inputs, the 102 mm circular burner using a propane reaction was represented using a square surface having 80 mm to simplify the geometry. Using the area of this surface (6 400 mm^2) with an assigned heat release rate per unit area of 2 109.4 kW m^{-2} yields an effective heat release rate of 13.5 kW for the burner, equivalent to that used within

the tests. To provide outputs for the model, gas phase devices representing thermocouples having the same assigned properties as those described in Section 5.4.1 were used to output calculated gas temperatures while, solid phase devices measuring adiabatic surface temperature were used to represent the CDPTs and surface thermocouples. The model outputs were configured to write to an Excel file each second, corresponding to the sampling rate for the devices used during the physical tests. A copy of the FDS source code used for the model is provided in Appendix A.

8.2 Sensitivity Analysis

When using numerical models, an important factor to consider is the balance between the accuracy/resolution of the calculated results and the physical time required for a computer to solve the model (wall-clock time). As part of finding this balance, a sensitivity analysis was completed comparing several models with varying mesh-resolutions against the wall-clock time for each arrangement.

To reduce overall wall-clock times, FDS can be configured to run using multi-thread processing, which allows individual meshes of the model to be calculated using separate logical processors within the computer cores. Since the computer used for the model had a total of 12 logical processors, the FDS model was split into 12 discrete meshes (one per logical processor) to take advantage of this functionality and maximize the efficiency of the computer in calculating the simulation results. As discussed in Section 8.1 and shown in Figure 37, these 12 discrete meshes were separated into two general areas: a high-resolution area (HRA) consisting of the mesh containing the burner and those directly

surrounding the NCTS (5 total), and a low-resolution area (LRA) consisting of the remaining meshes in the model.

An initial model was created with the meshes in the HRA (within 100 mm of the NCTS) having a grid size of 10 mm and those in the LRA having a grid size of 20 mm. This initial model took significantly longer than the others to solve. To improve wall-clock times on the initial model, the mesh refinement was reduced to having a 10 mm grid size in the HRA (within 40 mm of the NCTS) and a 40 mm grid size in the LRA. While this improved model did reduce the overall wall-clock times to approximately a third of the initial model, it was still found to take a significant amount of time to run. A final model was used having a 20 mm grid side in the HRA (within 40 mm of the NCTS) and a 40 mm grid size in the LRA. The results of the sensitivity analysis are presented in Table 5.

Table 5 Results of sensitivity analysis for the initial, improved, and final meshes.

Mesh	Grid Size (HRA)	Grid Size (LRA)	Total # of Cells	Estimated Wall-Clock Time to Calculate 300 s Model Time
Initial	10 mm	20 mm	315 580	367 200 s (approx. 102 h)
Improved	10 mm	40 mm	216 316	124 331 s (approx. 35 h)
Final	20 mm	40 mm	84 370	32 040 s (approx. 9 h)
Intel® Core™ i7-10750H CPU @ 2.60GHz, 2592 Mhz, 6 Cores, 12 Logical Processors				

As shown in Table 5, the final model used showed a significant reduction in the overall wall-clock times compared to the other mesh configurations explored. To provide insight into the accuracy of the final model, a comparison between the final model and the physical testing results has been provided in Section 8.3.

8.3 COMPARISON BETWEEN TESTING AND MODEL

To compare the results of the model against the physical testing results and to follow the approach used in Section 7.1.1, Figure 38 presents the observed temperatures for both the numerical and experimental results at a radius near, mid distance, and far away from the burner location over time.

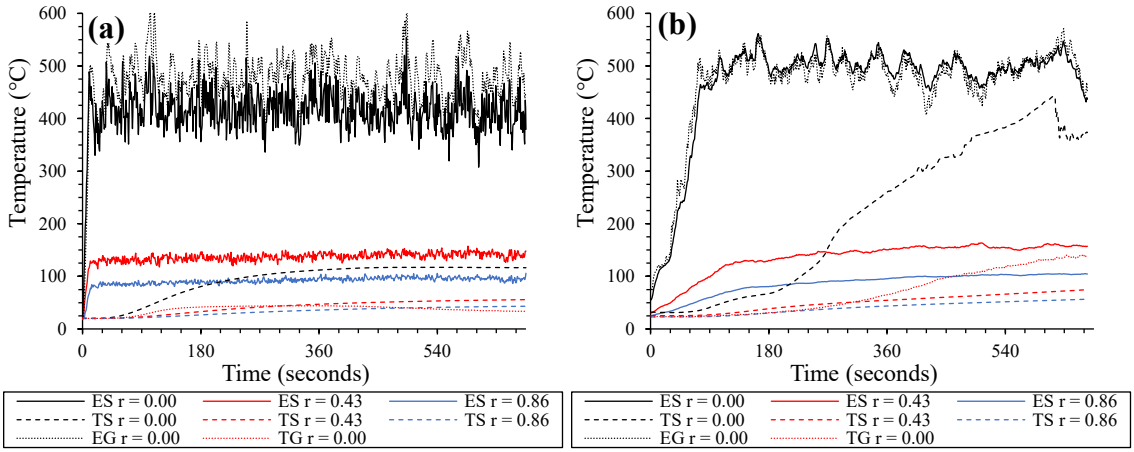

Figure 38 Temperatures observed in the (a) FDS model of Test #3 and (b) the physical results of Test #3.

The first impression received when comparing the results is that the modelled results have significantly more “noise” than the physical results. This could be attributed to variances in the model calculation and the capability to account for the thermal inertia of the model sampling probes. Next, it is noted that the model temperatures directly above the burner location reach a steady state almost immediately compared to the experimental test results, which took approximately 60 seconds to reach a steady state. The final impression is the discrepancy between the modeled and observed temperatures. The average model calculated and experimental surface temperatures after a time of 60 seconds (to isolate the transient stage of the experimental results) are provided in Table 6 and Table 7.

Table 6 Average model calculated surface temperatures after time of 60s.

Side of Tile	Radial Distance from Burner (m)	Mean $T_{Surface}$ (°C)	Standard Deviation (°C)
Exposed	0.0	497	28
	0.43	144	17
	0.86	92	13
Unexposed	0.0	239	135
	0.43	53	14
	0.86	41	10

Table 7 Average experimental surface temperatures after time of 60s.

Side of Tile	Radial Distance from Burner (m)	Mean $T_{Surface}$ (°C)	Standard Deviation (°C)
Exposed	0.0	417	35
	0.43	138	7
	0.86	93	5
Unexposed	0.0	99	25
	0.43	44	10
	0.86	34	7

As shown in Table 7, the model calculated mean surface temperature on the exposed side of the NCTS are approximately 80 °C lower than the physical testing results while the modelled temperatures on the at r = 0.43 m and r = 0.86 m appear to be comparable to those observed during the physical test. Regarding the temperatures on the unexposed side, a similar trend is observed in that the modelled temperatures at the burner location are significantly lower; however, in this case appeared to reach a steady state when compared to the experimental testing results. Furthermore, the modelled temperatures at r = 0.43 m and r = 0.86 m appear to be comparable to those observed during the physical test. The

difference between the trends of the modelled and observed temperatures can likely be attributed to the fact that the model assumes constant conditions for the NCTS and that it acts as an ideal isolating material, while in the physical test the NCTS would experience both moisture loss and degradation of the tile material; both conditions that would be more prominent directly above the burner location. Numerical accuracy may also be a contributing factor to these differences.

In addition to outputting the computed values from the model, FDS also has a built in visualization tool called Smokeview. While not perfectly accurate, the Smokeview software provides a visual representation of the model output for use by the model creator. Figure 40 provides an example of the output of the visualizer against the observed fire plume during Test 3.

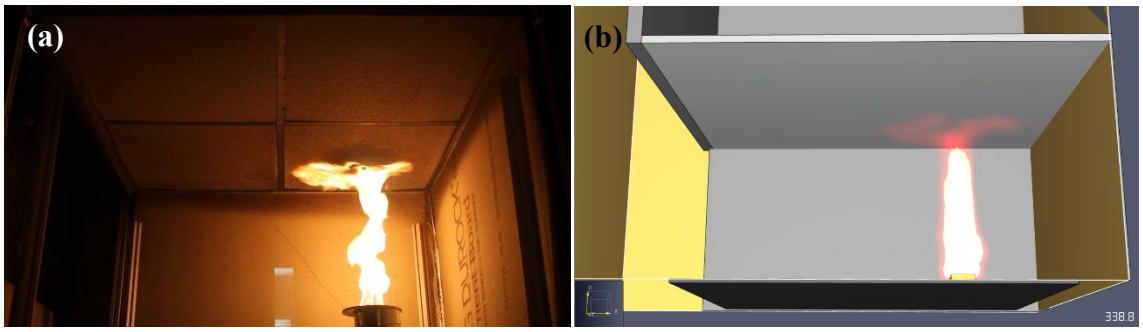

Figure 39 Comparison between (a) the observed fire plume during Test 3 and (b) visual representation of the visual fire plume as represented by Smokeview.

As can be seen in Figure 39, the Smokeview software provides a reasonable representation of the physical results with respect to the size of the flaming area and visible fire plume. While the results in Figure 38 and Figure 39 demonstrate that Test 3 can generally be represented using a numerical FDS model, these do not provide a means to measure the accuracy of each individual calculated value with respect to the observed temperatures. To

compare the accuracy of the model, the observed temperatures during Test 3 have been compared against the calculated temperature at each respective device location and individual time step in Figure 40.

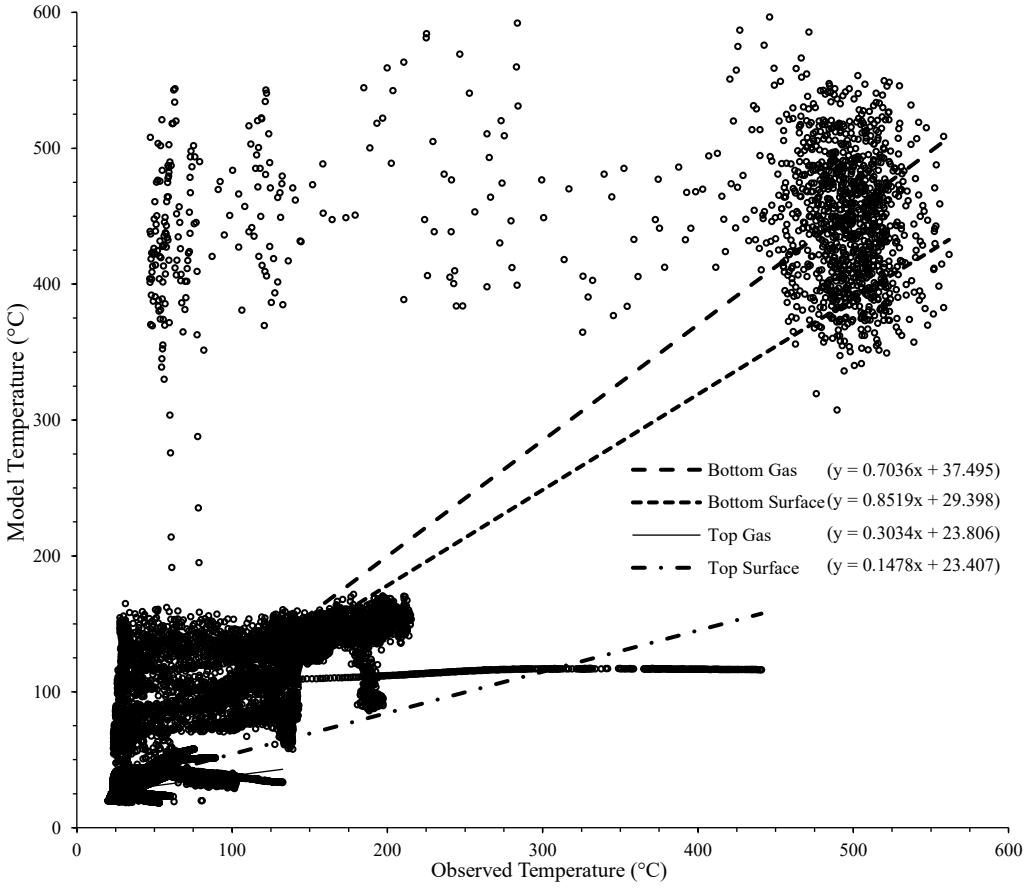

Figure 40 Model calculated temperatures plotted against the observed temperatures for Test #3. Trendlines are provided for each the surface and gas temperatures on both the exposed and unexposed sides.

Regarding the data provided within Figure 40, the linearity of the data points is considered to be the measure of the ability the model to predict the observed testing results. In this context, a slope greater than 1.0 represents the model over-predicting the temperatures observed during testing while a slope less than 1.0 indicates that the model under-predicts these temperatures. For each group of thermocouples noted (i.e., top gas/surface, bottom

gas/surface), the model was found to under-predict the observed temperatures, but there is a significant difference in the accuracy of the temperature predictions above and below the NCTS. On the exposed side the plots for the gas and surface temperatures had slopes of 0.704 and 0.852 respectively, compared to the plots for the gas and surface temperatures on the unexposed side which had slopes of 0.303 and 0.148 respectively. Based on this comparison, it is noted that the model appears to under-predict temperatures on the exposed side of the NCTS by approximately 15% to 30% and under-predict temperatures on the unexposed side of the NCTS by approximately 70% to 85%. This discrepancy in the accuracy of the modeled temperatures is likely attributed to the ability of the current model to represent the heat transfer from the gas-phase on the exposed side, to 1-D heat transfer through the NCTS, and then back to the gas-phase on the unexposed side of the NCTS.

Overall, it has been demonstrated that the model in its current configuration/resolution can be used to roughly approximate temperatures on the exposed side of the NCTS (with an error of approximately 15% to 30%); however, the current model does not provide an accurate representation of temperatures on the unexposed side of the NCTS. It is recommended that further research be completed to explore the ability of FDS represent the actual testing results on the unexposed side of the NCTS.

CHAPTER 9 CONCLUSIONS AND RECOMMENDATIONS

This section provides a summary of the results, analysis, and numerical validation completed in Chapters 7 and 8, and provides conclusions drawn based on the analysis completed therein. Recommendations for future research are also provided.

9.1 SUMMARY

The review provided in Section 7.1.1 provided an overview of the tests and observed temperatures, identified general issues encountered during the course of testing, and provided a handful of recommendations for topics and methods for future research. Trends regarding the failure of NCTSs including heat source location, ceiling height, and times to failure were analysed in Section 7.1.2, followed by a review of the endpoint condition of the tiles and apparent mode of failure in Section 7.1.3.

With respect to the thermal resistance provided prior to failure, Section 7.2.1 identified the average reduction in surface temperature between the exposed and unexposed sides of the NCTS and noted potential relationships between this value and the burner height and location. Similarly, Section 7.2.2 explored the average reduction in gas temperature between the exposed and unexposed sides of the NCTS and notes that overall, the reduction in average gas temperature tended to be larger than that of the surface temperature. The average rate of heat transfer through the NCTSs was explored in Section 7.2.3 and identified potential relationships between this and both the burner location and height.

Recommendations for the location of thermocouples in future research method were also provided.

Observed temperatures at the burner location for each test were analysed in Section 7.3, with the focus mainly being provided on surface temperatures at this location. This section identified both average temperatures on the fire-exposed side of the NCTS and the unexposed sides and identified needs for devices used in future research.

Chapter 8 provided a numerical validation for the testing results through the use of FDS. The FDS model was compared against the physical test results, as well as the capability of FDS to represent the observed fire plume. General trends from the results of the numerical model were identified, most notably that the model tended to underpredict observed temperatures. Limitations of the model in its current state are also identified in addition to recommending that future research be completed to explore the limits of FDS.

9.2 CONCLUSIONS

Overall, various conclusions can be drawn from the results of the testing ranging from failure modes of the NCTS to the ability of an FDS model to predict expected temperatures during a test. With respect to the individual aspects analysed in Chapters 7 and 8, the following conclusions are presented:

- When exposed to fire conditions, failure of the NCTS is expected to occur due to degradation of the tiles to the point that they can no longer support their own weight.
- The average time to failure for the NCTS during testing was found to be 680 seconds with an expected time to failure (at a 95% confidence) between 477 and 901 seconds.
- Average surface and gas temperature reductions of 134°C and 195°C respectively were observed across the entire NCTS between the exposed and unexposed sides.
- Prior to failure (i.e., at a time of 477 seconds), the average rate of heat transfer through the NCTS was found to be 0.752 kW; equivalent to approximately 5.57% of the total heat release rate (13.5 kW) of the burner.
- At the location of the burner at the time to failure, the average surface temperature on the fire-exposed side of the NCTS was observed to be 560°C with an average temperature reduction of 223°C between the exposed and unexposed sides of the NCTS.
- The FDS model in its current configuration can be used to roughly approximate temperatures on the exposed side of the NCST, however modelled temperatures tended to be approximately 15–30% lower than the actual expected results.

Extrapolating from the above individual conclusions, it is finally concluded that: when the NCTS were exposed to temperatures on the order of 560°C, they can be expected to remain

in place for a period of at least 477 seconds and while remaining in place, provide a reduction in the observed surface temperature between the exposed and unexposed sides of approximately 223°C at the fire location. It is noted however that this research did not take into consideration scalability if the tests, the impact of fixtures located in an NCTS, and the effect of forces exerted on the NCTS by a buoyant fire plume.

9.3 RECOMMENDATIONS

Further to the conclusions presented in Section 9.2 based on the outcomes of the testing process, various recommendations have been identified for consideration in any future research. With respect to the methods employed during future research, the following is recommended that:

- Future research using propane as a heat source employ the use of multiple propane tanks manifolded together,
- Future research should explore additional options for measuring surface temperatures on the unexposed side of the NCTS, and
- Future research should consider the use of gas-phase thermocouples located directly above the burner location for each testing scenario.

Various potential trends were observed throughout the research process for consideration in future research however these were not explored at this point. Specifically, the following areas for future research have been identified:

- The impact of the burner proximity to the apparatus walls on the observed ceiling tile temperatures.
- The impact of the height between the burner and the NCTS on both the time to failure and the reduction in temperature across the NCTS.
- The apparent relation between the size of the charred area of the NCTS and the burner height.
- The impact of the burner location and height between the burner and the NCTS on the calculated rate of heat transfer through the NCTS.
- The ability of FDS to represent the observed testing results, specifically expected temperatures on the unexposed side of the NCTS.

In addition to the above trends identified for future research, it is noted that additional research should be completed to explore the scalability of the testing results on a full-size room fire with a NCTS installed. Any such research on the scalability of these results should also consider the impact of fixtures (such as lighting or air diffusers) located in the plane of the NCTS and the impact of forces exerted on the NCTS from a buoyant fire plume.

REFERENCES

[1] Canadian Commission on Building and Fire Codes, National Building Code of Canada, National Research Council, 2015.

[2] ASTM International, ASTM E119 Standard Test Methods for Fire Tests of Building Construction and Materials, West Conshohocken: ASTM International, 2018.

[3] Parliament of England, An Act for the Rebuilding of London, London: City of London Corporation, 1667.

[4] International Code Council, International Building Code, International Codes, 2018.

[5] National Fire Protection Association, NFPA 101 Life Safety Code, National Fire Protection Association, 2021.

[6] Society of Fire Protection Engineers, The SFPE Guide to Performance-Based Fire Safety Design, Society of Fire Protection Engineers, 2015.

[7] National Institute of Standards and Technology, "Fire Dynamics Simulator (FDS) and Smokeview (SMV)," National Institute of Standards and Technology, [Online]. Available: https://pages.nist.gov/fds-smv/downloads.html. [Accessed 20 October 2020].

[8] National Institute of Standards and Technology, Fire Dynamics Simulator Technical Reference Guide Volume 1: Mathematical Model, National Institute of Standards and Technology, 2020.

[9] RJ Bartlett Engineering Ltd., "12070 Final FPE Analysis R140327," RJ Bartlett Engineering Ltd., Fredericton, 2014.

[10] National Institute of Standards and Technology, "Fire Dynamics Simulator User's Guide," National Institute of Standards and Technology, 2019.

[11] ASTM International, ASTM E84 Standard Test Method for Surface Burning Characteristics of Building Materials, West Conshohocken: ASTM International, 2018.

[12] F. L. Brannigan, "SUSPENDED CEILINGS," vol. 158, no. 4, 2005.

[13] V. P. R. Babrauskas, "Heat Release Rate: The Single Most Important Variable in Fire Hazard," 1991.

[14] ASTM International, "ASTM E906 Standard Test Method for Heat and Visible Smoke Release Rates for Materials and Products," American Society for Testing and Materials, Philadelphia, 1983.

[15] ASTM International, ASTM E1354 -16a Standard Test Method for Heat and Visible Smoke Release Rates for Materials and Products using an Oxygen Consumption Calorimeter, West Conshohocken: ASTM International, 2016.

[16] International Organization for Standardization, "ISO 5660 Fire Tests - Reaction to Fire - Part 1: Rate of Heat Release from Burning Products," International Standards Organization, Geneva, 1993.

[17] C. E. Baukal and B. Gebhart, "Surface Condition Effects on Flame Impingement Heat Transfer," *Experimental Thermal and Fluid Science,* vol. 15, pp. 323-335, 1997.

[18] L. Hu, L. Chen and W. Tang, "A global model on temperature profile of buoyant ceiling gas flow in a channel with combining mass and heat loss due to ceiling extraction and longitudinal forced air flow," *International Journal of Heat and Mass Transfer,* vol. 79, pp. 885-892, 2014.

[19] S. Li, R. Zong, W. Zhao, Z. Yan and G. Liao, "Theoretical and experimental analysis of ceiling-jet flow in corridor fires," *Tunnelling and Underground Space Technology,* vol. 26, pp. 651-658, 2011.

[20] M. Remie, M. Cremers, K. Schreel and L. de Goey, "Analysis of the heat transfer of an impinging laminar flame jet," *International Journal of Heat and Mass Transfer,* vol. 50, pp. 2816-2827, 2007.

[21] S. Chander and A. Ray, "Flame impingement heat transfer: A review," *Energy Conversion and Management,* vol. 46, p. 2803, 2005.

[22] H. Ding and J. Quintiere, "An integral model for turbulent flame radial lengths under a ceiling," *Fire Safety Journal,* vol. 52, pp. 25-33, 2012.

[23] M. A. Kokkala, "Experimental Study of Heat Transfer to Ceiling from an Impinging Diffusion Flame," International Association for Fire Safety Science, Espoo, Finland, 1991.

[24] D. Drysdale, "An Introduction to Fire Dynamics, 3rd Edition," Wiley, 2011.

[25] R. Alpert, "Calculation of Response Time of Ceiling Mounted Fire Detectors," Philadelphia, 1972.

[26] T. Bergman, A. Lavine, F. Incropera and D. Dewitt, Fundamentals of Heat and Mass Transfer, Hoboken: Wiley, 2011.

[27] H. S. D. b. M. B. Michael Moran, Fundamentals of Engineering Thermodynamics, Eighth Edition, Wiley, 2014.

[28] U. Wickstrom, "Adiabatic Surface Temperature and the Plate Thermometer for Calculating Heat Transfer and Controlling Fire Resistance Furnaces," Fire Safety Science-Proceedings of the Ninth International Symposium, Boras, 2008.

[29] A. Robbins, "Plate Thermometers for Measuring Heat Transfer," Build Fire Safety, 2009.

[30] U. Wickstrom, Temperature Calculation in Fire Safety Engineering, Chapter 9.3.3 Alternative Plate Thermometer Designs, Springer International Publishing Switzerland, 2016.

[31] USG, "Safety Data Sheet Armstrong (R) Mineral Fiber Acoustical Ceiling Tiles and Wall Panels," Armstrong Ceilings, Lancaster, 2013.

[32] L. I. D. Bergman, Fundamentals of Heat and Mass Transfer Seventh Edition, Hoboken: Wiley, 20018.

[33] J. L. Thomason, U. Nagel, L. Yang and D. Bryce, "A study of the thermal degradation of glass fibre sizings at composite processing temperatures," *Composites Part A: Applied Science and Manufacturing,* vol. 121, pp. Pages 56-63, 2019.

[34] Thunderhead Engineering, "PryoSim," Thunderhead Engineering, Manhattan, 2021.

APPENDIX A FDS SOURCE CODE

```
&MESH ID='MESH-a-a-a', IJK=18,15,14, XB=0.0,0.72,0.0,0.6,-0.1,0.46/
&MESH ID='MESH-a-a-b', IJK=18,16,14, XB=0.0,0.72,0.6,1.24,-0.1,0.46/
&MESH ID='MESH-a-b-a-a', IJK=36,30,4, XB=0.0,0.72,0.0,0.6,0.46,0.54/
&MESH ID='MESH-a-b-a-b', IJK=36,32,4, XB=0.0,0.72,0.6,1.24,0.46,0.54/
&MESH ID='MESH-a-b-b-a', IJK=18,15,15, XB=0.0,0.72,0.0,0.6,0.54,1.14/
&MESH ID='MESH-a-b-b-b', IJK=18,16,15, XB=0.0,0.72,0.6,1.24,0.54,1.14/
&MESH ID='MESH-b-a-a', IJK=20,15,14, XB=0.72,1.52,0.0,0.6,-0.1,0.46/
&MESH ID='MESH-b-a-b', IJK=40,32,28, XB=0.72,1.52,0.6,1.24,-0.1,0.46/
&MESH ID='MESH-b-b-a-a', IJK=40,30,4, XB=0.72,1.52,0.0,0.6,0.46,0.54/
&MESH ID='MESH-b-b-a-b', IJK=40,32,4, XB=0.72,1.52,0.6,1.24,0.46,0.54/
&MESH ID='MESH-b-b-b-a', IJK=20,15,15, XB=0.72,1.52,0.0,0.6,0.54,1.14/
&MESH ID='MESH-b-b-b-b', IJK=20,16,15, XB=0.72,1.52,0.6,1.24,0.54,1.14/

&REAC ID='Propane',
    FUEL='REAC_FUEL',
    FORMULA='C3H8',
    AUTO_IGNITION_TEMPERATURE=0.0/

&DEVC ID='LFBG', QUANTITY='THERMOCOUPLE', XYZ=0.6,0.3,0.48/
&DEVC ID='LRBG', QUANTITY='THERMOCOUPLE', XYZ=0.6,0.92,0.48/
&DEVC ID='RFBG', QUANTITY='THERMOCOUPLE', XYZ=1.22,0.3,0.48/
&DEVC ID='RRBG', QUANTITY='THERMOCOUPLE', XYZ=1.22,0.92,0.48/
&DEVC ID='RRTG', QUANTITY='THERMOCOUPLE', XYZ=1.22,0.92,0.54/
&DEVC ID='LFTG', QUANTITY='THERMOCOUPLE', XYZ=0.6,0.3,0.54/
&DEVC ID='LRTG', QUANTITY='THERMOCOUPLE', XYZ=0.6,0.92,0.54/
&DEVC ID='RFTG', QUANTITY='THERMOCOUPLE', XYZ=1.22,0.3,0.54/
&DEVC ID='LFB3', QUANTITY='ADIABATIC SURFACE TEMPERATURE', XYZ=0.34,0.02,0.5, IOR=-3/
&DEVC ID='LRB3', QUANTITY='ADIABATIC SURFACE TEMPERATURE', XYZ=0.34,1.2,0.5, IOR=-3/
&DEVC ID='RRB3', QUANTITY='ADIABATIC SURFACE TEMPERATURE', XYZ=1.5,1.2,0.5, IOR=-3/
&DEVC ID='RFB3', QUANTITY='ADIABATIC SURFACE TEMPERATURE', XYZ=1.5,0.02,0.5, IOR=-3/
&DEVC ID='LFB2', QUANTITY='ADIABATIC SURFACE TEMPERATURE', XYZ=0.6,0.3,0.5, IOR=-3/
&DEVC ID='LRB2', QUANTITY='ADIABATIC SURFACE TEMPERATURE', XYZ=0.6,0.92,0.5, IOR=-3/
&DEVC ID='RRB2', QUANTITY='ADIABATIC SURFACE TEMPERATURE', XYZ=1.22,0.92,0.5, IOR=-3/
&DEVC ID='RFB2', QUANTITY='ADIABATIC SURFACE TEMPERATURE', XYZ=1.22,0.3,0.5, IOR=-3/
&DEVC ID='LFB1', QUANTITY='ADIABATIC SURFACE TEMPERATURE', XYZ=0.88,0.58,0.5, IOR=-3/
&DEVC ID='LRB1', QUANTITY='ADIABATIC SURFACE TEMPERATURE', XYZ=0.88,0.64,0.5, IOR=-3/
&DEVC ID='RFB1', QUANTITY='ADIABATIC SURFACE TEMPERATURE', XYZ=0.94,0.58,0.5, IOR=-3/
&DEVC ID='RRB1', QUANTITY='ADIABATIC SURFACE TEMPERATURE', XYZ=0.94,0.64,0.5, IOR=-3/
&DEVC ID='LFT3', QUANTITY='WALL TEMPERATURE', XYZ=0.34,0.02,0.52, IOR=3/
&DEVC ID='LRT3', QUANTITY='WALL TEMPERATURE', XYZ=0.34,1.2,0.52, IOR=3/
&DEVC ID='RRT3', QUANTITY='WALL TEMPERATURE', XYZ=1.5,1.2,0.52, IOR=3/
&DEVC ID='RFT3', QUANTITY='WALL TEMPERATURE', XYZ=1.5,0.02,0.52, IOR=3/
&DEVC ID='LFT2', QUANTITY='WALL TEMPERATURE', XYZ=0.6,0.3,0.52, IOR=3/
&DEVC ID='LRT2', QUANTITY='WALL TEMPERATURE', XYZ=0.6,0.92,0.52, IOR=3/
&DEVC ID='RRT2', QUANTITY='WALL TEMPERATURE', XYZ=1.22,0.92,0.54, IOR=3/
&DEVC ID='RFT2', QUANTITY='WALL TEMPERATURE', XYZ=1.22,0.3,0.52, IOR=3/
&DEVC ID='LFT1', QUANTITY='WALL TEMPERATURE', XYZ=0.88,0.58,0.54, IOR=3/
&DEVC ID='LRT1', QUANTITY='WALL TEMPERATURE', XYZ=0.88,0.64,0.54, IOR=3/
&DEVC ID='RFT1', QUANTITY='WALL TEMPERATURE', XYZ=0.94,0.58,0.54, IOR=3/
&DEVC ID='RRT1', QUANTITY='WALL TEMPERATURE', XYZ=0.94,0.64,0.54, IOR=3/

&MATL ID='Tile',
    SPECIFIC_HEAT=1.34,
    CONDUCTIVITY=0.058,
    DENSITY=208.0/
```

```
&SURF ID='ADIABATIC',
    COLOR='GRAY 80',
    ADIABATIC=.TRUE./
&SURF ID='Ceiling Tile',
    COLOR='WHITE',
    MATL_ID(1,1)='Tile',
    MATL_MASS_FRACTION(1,1)=1.0,
    THICKNESS(1)=0.0125/
&SURF ID='Heat Source',
    COLOR='RED',
    HRRPUA=2109.4,
    RAMP_Q='Heat Source_RAMP_Q',
    TMP_FRONT=300.0/
&RAMP ID='Heat Source_RAMP_Q', T=0.0, F=0.0/
&RAMP ID='Heat Source_RAMP_Q', T=10.0, F=1.0/

&OBST ID='Obstruction', XB=0.32,1.525,0.0,1.22,0.5,0.52, THICKEN=.TRUE., SURF_IDS='Ceiling
Tile','ADIABATIC','Ceiling Tile'/
&OBST ID='CementBoard_Xmin', XB=0.28,0.32,0.0,1.24,0.5,1.14, COLOR='GRAY 60', SURF_ID='INERT'/
&OBST ID='Platform', XB=0.405,1.425,0.1,1.12,-0.1,-0.09, COLOR='GRAY 40', SURF_ID='INERT'/
&OBST ID='CementBoard_Xmax', XB=1.52,1.525,0.0,1.22,-0.1,1.11, COLOR='GRAY 60', SURF_ID='INERT'/
&OBST ID='CementBoard_Ymax', XB=0.305,1.525,1.215,1.22,-0.1,1.11, COLOR='GRAY 60',
SURF_ID='INERT'/
&OBST ID='CementBoard_Ymin', XB=0.305,1.525,0.0,5.0E-3,-0.1,1.11, COLOR='INVISIBLE',
SURF_ID='INERT'/
&OBST ID='CementBoard_Zmax', XB=0.305,1.525,0.0,1.22,1.105,1.11, COLOR='GRAY 60',
SURF_ID='INERT'/
&OBST ID='BurnerPlate', XB=1.18,1.26,0.88,0.96,-0.09,0.0, SURF_IDS='Heat Source','INERT','INERT'/

&VENT ID='Mesh Vent: MESH-a-a [ZMIN]', SURF_ID='OPEN', XB=0.0,0.72,0.0,1.24,-0.1,-0.1/
&VENT ID='Mesh Vent: MESH-a-b-b [ZMAX]', SURF_ID='OPEN', XB=0.0,0.72,0.0,1.24,1.14,1.14/
&VENT ID='Mesh Vent: MESH-b-a [ZMIN]', SURF_ID='OPEN', XB=0.72,1.56,0.0,1.24,-0.1,-0.1/
&VENT ID='Mesh Vent: MESH-b-b-b [ZMAX]', SURF_ID='OPEN', XB=0.72,1.56,0.0,1.24,1.14,1.14/

&SLCF QUANTITY='TEMPERATURE', VECTOR=.TRUE., XB=0.0,1.525,0.0,1.22,-0.1,1.11,
FYI='Temperature'/

&Tail /
```